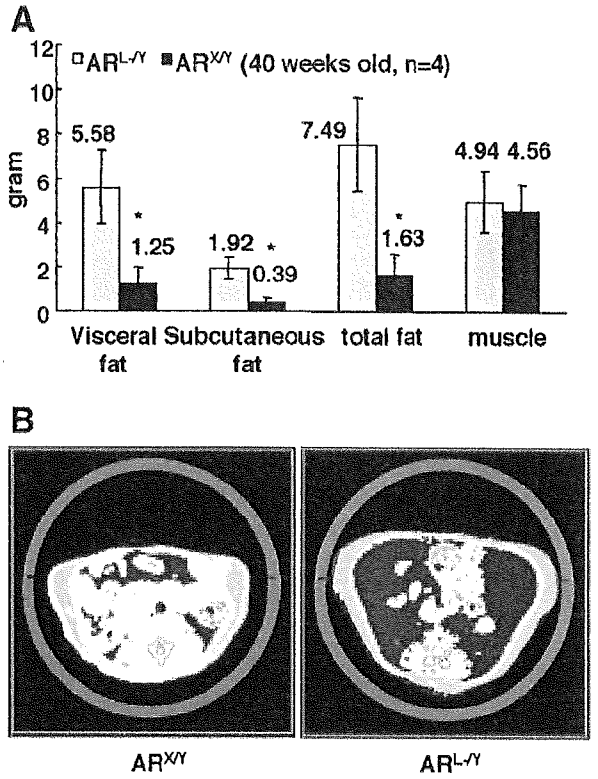

FIG. 1. CT-based body composition analysis of 40-week-old $AR^{L-/Y}$ and $AR^{X/Y}$ mice. *A*: CT-estimated amounts of visceral fat, subcutaneous fat, and muscle in the abdominal area of L2–L4. *B*: Representative CT images of $AR^{X/Y}$ (*left*) and $AR^{L-/Y}$ (*right*) mice at the L3 level. The pink and yellow areas represent the visceral and subcutaneous fat, respectively. *$P < 0.01$ compared with $AR^{L-/Y}$, $n = 4$.

$AR^{L-/Y}$ mice were significantly smaller than those of $AR^{X/Y}$ mice (Fig. 2*B*), supporting previous studies demonstrating smaller kidneys in orchidectomized mice (16,17).

In comparison to $AR^{X/Y}$ mice, subcutaneous WAT from $AR^{L-/Y}$ mice was hypertrophic (Figs. 2*C* and *D*). The interscapular BAT in $AR^{L-/Y}$ mice was relatively enlarged and pale (Fig. 2*E*), and it contained higher lipid content (Figs. 2*F* and *G*). A considerable number of cells in $AR^{L-/Y}$ BAT were large and contained unilocular lipid deposits that morphologically mimicked WAT adipocytes (data not shown). Leptin transcript, which is normally restricted to WAT, was elevated in $AR^{L-/Y}$ WAT, as expected (Fig. 2*H*). However, it was also elevated in $AR^{L-/Y}$ BAT (Fig. 2*I*), suggesting that BAT from $AR^{L-/Y}$ mice has characteristics of both BAT and WAT. Thus the BAT of $AR^{L-/Y}$ mice is similar to that from mice in which the genes encoding all three β-adrenergic receptors have been inactivated (18). Despite the apparent obesity, $AR^{L-/Y}$ mice manifested no evidence of fatty liver (data not shown), which is a common consequence of obesity. Because estrogen deficiency has been found to increase WAT in male mice (19,20), and estrogen can be produced by aromatizing testosterone (21), which is severely decreased in $AR^{L-/Y}$ mice because of atrophic testis (12), we addressed the issue of estrogen levels in $AR^{L-/Y}$ mice. We previously reported that at 8 weeks old, before the onset of obesity, serum E2 in $AR^{L-/Y}$ mice was normal (12). In the present study, we found that E2 levels in $AR^{L-/Y}$ mice at 40 weeks of age are still indistinguishable from those in $AR^{X/Y}$ mice (Fig. 2*J*), suggesting $AR^{L-/Y}$ mice are not in short supply of estrogen.

Serum levels of total protein (5.1 ± 0.61 g/dl in $AR^{X/Y}$ mice vs. 4.8 ± 0.9 g/dl in $AR^{L-/Y}$ mice, $n = 6$, $P = 0.49$), blood urea nitrogen (26.5 ± 4.6 mg/dl in $AR^{X/Y}$ vs. 20.8 ± 7.2 g/dl in $AR^{L-/Y}$ mice, $n = 6$, $P = 0.12$), and glucose (78.5 ± 14.2 mg/dl in $AR^{X/Y}$ vs. 88.0 ± 9.9 mg/dl in $AR^{L-/Y}$ mice, $n = 6$, $P = 0.26$) were found unchanged. Those of triglycerides, unesterified free fatty acids, and total cholesterol were also unchanged (10). Serum insulin in $AR^{L-/Y}$ mice tended to be slightly higher, but it did not reach statistical significance (Fig. 3*A*). Unexpectedly, we observed a significant increase in serum adiponectin concentration in $AR^{L-/Y}$ mice (Fig. 3*B*). Adiponectin sensitizes insulin sensitivity via various mechanisms (13,22), and its plasma concentration is negatively correlated with obesity. The unique hyperadiponectinemia in $AR^{L-/Y}$ mice thus prompted us to further evaluate the overall insulin sensitivity. Insulin challenge tests and intraperitoneal glucose tolerance tests were performed on 40-week-old mice. Neither test revealed any differences between the two groups (Figs. 3*C* and *D*), suggesting that overall insulin sensitivity remained intact in $AR^{L-/Y}$ mice, despite their apparent obesity. In contrast to the elevated plasma level of adiponectin, the adiponectin transcript was strikingly decreased in the WAT of obese $AR^{L-/Y}$ mice (Fig. 3*E*), as is commonly observed with obesity. The adiponectin transcript levels were found to be unchanged in $AR^{L-/Y}$ BAT (Fig. 3*F*), ruling out the possibility that BAT, though WAT-like, is an additional adiponectin source. We next carried out CT-based body composition analysis for the whole body to evaluate the relative WAT mass (%WAT) at the whole-body level (%WAT = 100% × whole-body WAT [g]/body weight [g]), and we subsequently estimated the relative total adiponectin production, using the equation: RTAP = %WAT × RAT, where RTAP is the relative total adiponectin production, and RAT is the relative adiponectin transcript copies to β-actin. As shown in Fig. 3*G*, although not statistically different, relative total adiponectin production from $AR^{L-/Y}$ mice was still lower than that from $AR^{X/Y}$ mice. Thus the discordance of adiponectin serum levels and adiponectin transcript levels in WAT still exists because serum adiponectin levels in $AR^{X/Y}$ mice were almost doubled (Fig. 3*B*). Collectively, these data suggest that the intact androgen-AR system of $AR^{X/Y}$ mice is suppressive to the secretion of adiponectin from WAT, whereas $AR^{L-/Y}$ mice had relatively enhanced secretion of the adipokine. In addition to hyperadiponectinemia, we also observed a significant reduction of peroxisome proliferator–activated receptor-γ (PPAR-γ) mRNA in the WAT of $AR^{L-/Y}$ compared with $AR^{X/Y}$ mice (Fig. 3*H*), which might also contribute to the normal insulin sensitivity of $AR^{L-/Y}$ mice (23).

We then studied the molecular events of glucose metabolism in skeletal muscle because muscle is a major target of androgen and adiponectin as well. As shown in Fig. 3*I–M*, although GLUT1 transcript levels were unchanged (data not shown), GLUT4 (muscle-dominant type) levels in $AR^{L-/Y}$ mice were significantly upregulated. The muscle-dominant hexokinase I was also upregulated, although no change was found for hexokinase II. Muscle-type phosphofructokinase tended, albeit not statistically significantly, to

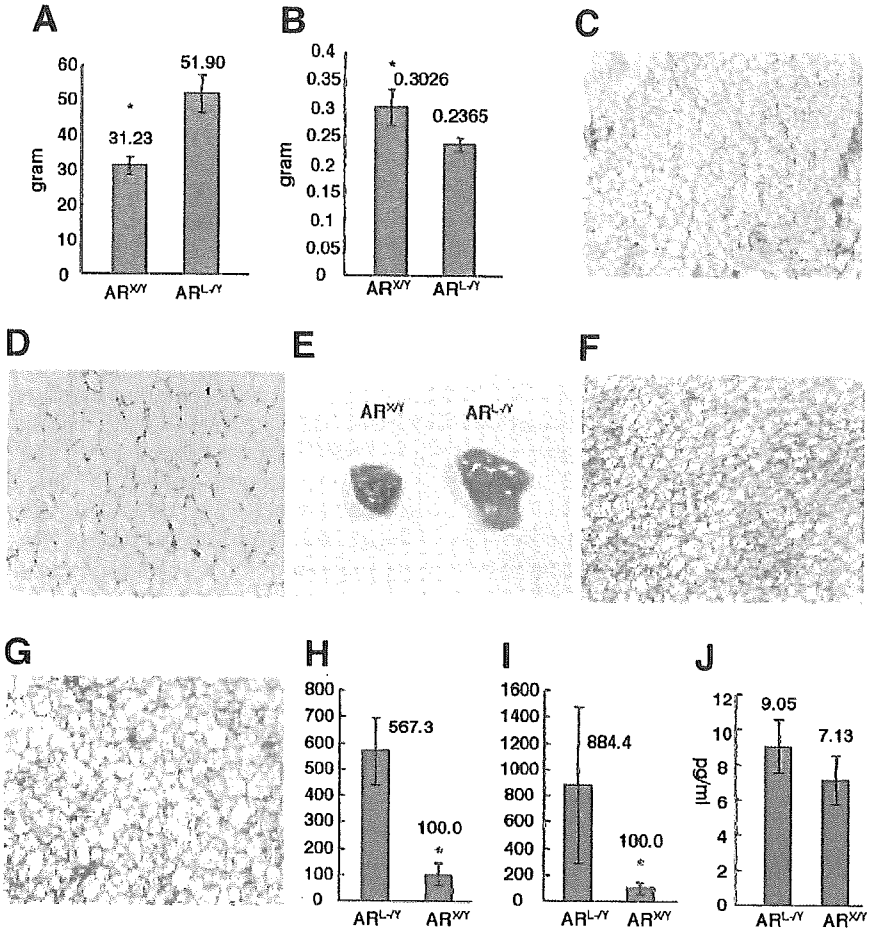

FIG. 2. General characteristics of late-onset obesity in $AR^{L-/Y}$ mice. *A*: Body weights of 45-week-old $AR^{L-/Y}$ and $AR^{X/Y}$ mice (n = 6). *B*: Kidney weights of 45-week-old $AR^{L-/Y}$ and $AR^{X/Y}$ mice (n = 6). *C* and *D*: The subcutaneous WAT of $AR^{X/Y}$ (*C*) and $AR^{L-/Y}$ mice (*D*), respectively (magnification 100×); it was hypertrophic in $AR^{L-/Y}$ compared with in $AR^{X/Y}$ mice. *E–G*: Interscapular BAT in $AR^{X/Y}$ (*F*) and $AR^{L-/Y}$ mice (*G*); it was enlarged and pale in $AR^{L-/Y}$ compared with in $AR^{X/Y}$ mice (magnification 100× in *F* and *G*). *H* and *I*: Leptin transcript levels in WAT (*H*) and BAT (*I*) in $AR^{X/Y}$ and $AR^{L-/Y}$ mice. The transcript levels in $AR^{X/Y}$ were set at 100. *J*: Serum E2 levels in $AR^{L-/Y}$ and $AR^{X/Y}$ mice. *$P < 0.01$ compared with $AR^{L-/Y}$ mice, n = 6.

be higher, whereas increase in muscle-type pyruvate kinase (including muscle-type pyruvate kinase-1 and -2) reached statistical significance. These data suggest glucose uptake and oxidation in muscle might be activated in $AR^{L-/Y}$ mice.

The concept of energy balance, which comprises both energy intake (feeding) and energy expenditure (physical activity, basal metabolism, and adaptive thermogenesis), is the key to understanding obesity (24). We first found that ad libitum food intake was unchanged between $AR^{L-/Y}$ and $AR^{X/Y}$ mice; that is, $AR^{L-/Y}$ mice were euphagic, as already reported (10). Next, we measured spontaneous physical activity for mice at around 8, 20, and 40 weeks of age (Table 2). During the 8-h monitoring period while the lights were off, the 20-week-old $AR^{L-/Y}$ mice ran a significantly shorter distance and showed almost half the number of rearing (standing up on hind legs) behaviors, another important parameter of dynamic behavior, as compared with $AR^{X/Y}$ mice. $AR^{L-/Y}$ mice also showed decreased activity at 40 weeks of age and, importantly, at 8 weeks of age, when the body weight of $AR^{L-/Y}$ mice had not yet exceeded that of $AR^{X/Y}$ mice. This suggests that the reduced activity of $AR^{L-/Y}$ mice is an intrinsic defect but not a secondary effect of the mice being overweight.

For the metabolic rate assessment, we first ensured that the thyroid functions of the two groups were comparable. Both serum thyrotropin (6.67 ± 3.67 ng/ml in $AR^{L-/Y}$ mice vs. 8.22 ± 2.05 ng/ml in $AR^{X/Y}$ mice, n = 6, $P > 0.05$) and 3,5,3′-triiodothyronine (0.58 ± 0.18 ng/ml in $AR^{L-/Y}$ mice versus 0.50 ± 0.11 ng/ml in $AR^{X/Y}$ mice, n = 6, $P > 0.05$) were unchanged. The rectal temperatures of both groups of mice at 22 weeks of age at room temperature were similar (37.97 ± 0.46°C in $AR^{L-/Y}$ mice vs. 38.40 ± 0.43°C in $AR^{X/Y}$ mice, $P > 0.05$). We next compared the overall oxygen consumption ratio by indirect calorimetry. To minimize interference effects of the activity differences between the two groups of mice on the Vo_2 results, we housed the mice for calorimetry in chambers of 10 × 20 cm^2, which were less than one-tenth the size of the infrared frames (45 × 45 cm^2) used to monitor the spontaneous activities. Figure 4*A* shows representative oxygen consumption (Vo_2) curves of one pair of $AR^{L-/Y}$ and $AR^{X/Y}$ mice. It is apparent that besides the average level, both peaks and troughs of the curves, which represent periods of movement and resting, respectively, are generally lower in $AR^{L-/Y}$ mice. Figure 4*B* summarizes the average mean Vo_2; $AR^{L-/Y}$ mice consumed ~30% less oxygen than $AR^{X/Y}$ mice. These data collectively indicate that $AR^{L-/Y}$ mice had a positive energy balance, which favors the onset of obesity (25). To analyze the molecular mechanisms of the increased adiposity, we applied real-time PCR to determine the transcript levels of various genes involved in thermoregulation and lipid metabolism in WAT and BAT.

In the WAT of $AR^{L-/Y}$ mice, the expression level of the most important thermogenetic molecule, UCP-1 (26), was less than one-tenth of that in $AR^{X/Y}$ mice (Fig. 5*A*). AR is possibly a novel positive regulator of the UCP-1 gene

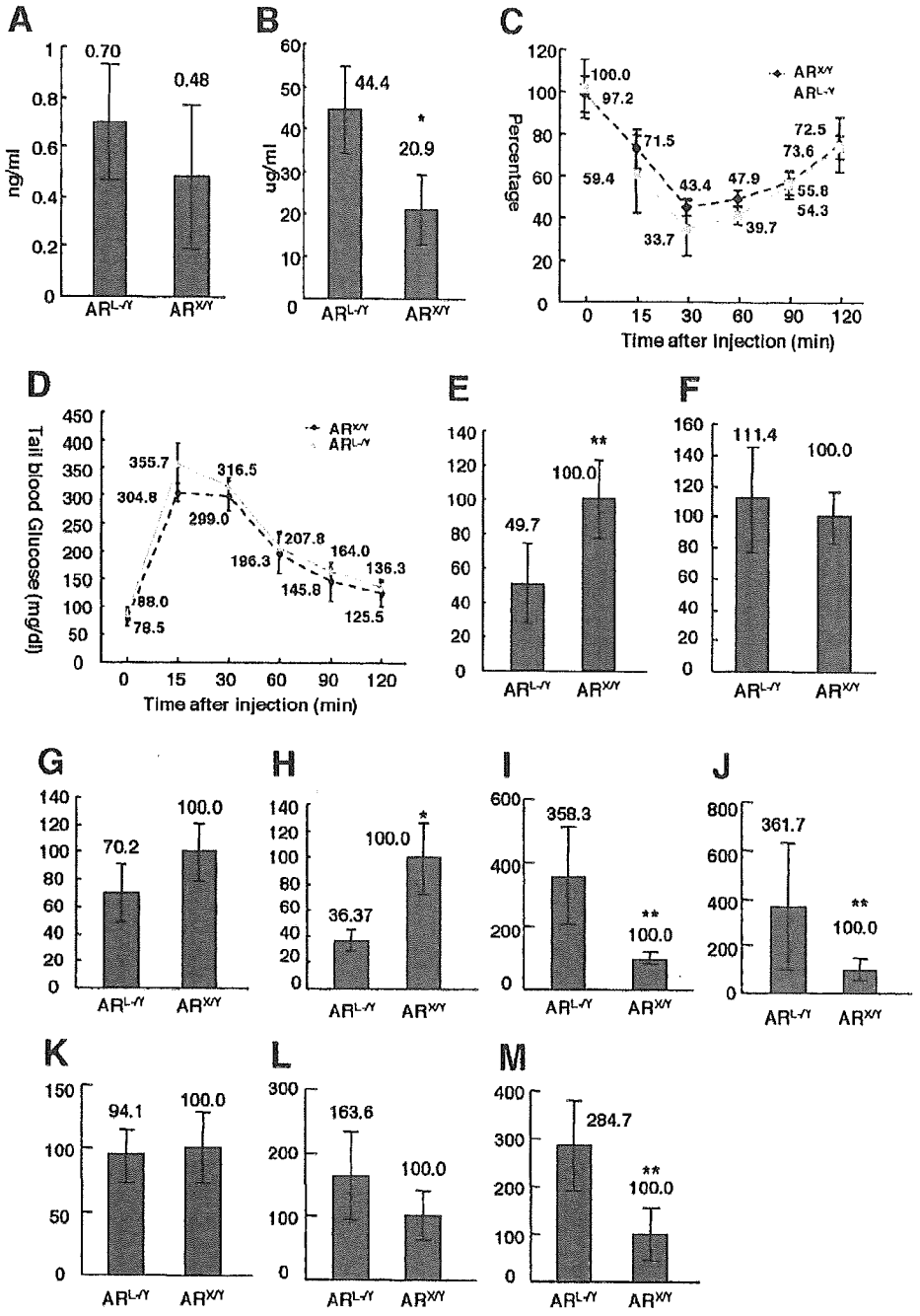

FIG. 3. Enhanced adiponectin release from WAT and intact insulin sensitivity. *A*: Serum insulin levels in $AR^{L-/Y}$ and $AR^{X/Y}$ mice. *B*: Serum adiponectin levels in $AR^{L-/Y}$ and $AR^{X/Y}$ mice. *C*: Results of the insulin challenge test; 0.7 units regular insulin/kg body wt i.p. was injected into $AR^{L-/Y}$ and $AR^{X/Y}$ mice after overnight fasting. Tail blood glucose levels were monitored at the indicated time points. The initial glucose levels in $AR^{L-/Y}$ mice were set at 100%. *D*: Results of the intraperitoneal glucose tolerance test; 2 g D-glucose/kg body wt i.p. was injected into $AR^{L-/Y}$ and $AR^{X/Y}$ mice after overnight fasting. Tail blood glucose levels were monitored at the indicated time points. Note that there was no apparent difference in overall insulin sensitivity. *E* and *F*: Transcript levels of WAT (*E*) and BAT (*F*) adiponectin in $AR^{L-/Y}$ and $AR^{X/Y}$ mice. $AR^{X/Y}$ values were set at 100. *G*: Estimated relative total adiponectin production (RTAP) in $AR^{L-/Y}$ and $AR^{X/Y}$ mice; RTAP = %WAT × RAT, where %WAT = 100% × whole-body WAT (g)/body wt (g), and RAT is the relative adiponectin transcript copies to β-actin. $AR^{X/Y}$ values were set at 100. *H*: Transcript levels of WAT PPAR-γ in $AR^{L-/Y}$ and $AR^{X/Y}$ mice. $AR^{X/Y}$ values were set at 100. *I–M*: Transcript levels of skeletal muscle GLUT4 (*I*), hexokinase I (*J*), hexokinase II (*K*), muscle-type phosphofructokinase (*L*), and muscle-type pyruvate kinase (*M*), respectively, in both groups of mice. $AR^{X/Y}$ values were set at 100. $^*P < 0.01$; $^{**}P < 0.05$ compared with $AR^{L-/Y}$ mice ($n = 6$, except *G*, in which $n = 4$).

because we revealed three steroid receptor response elements (TGTTCT) on a UCP-1 promoter sequence (up to −7,645 bp, GenBank accession no. U63418), and a 3.85-kb UCP-1 promoter, which contains the last consensus sequence, positively responded to AR in NIH-3T3-L1 adipocytes in a dihydrotestosterone-dependent manner (Fig. 5*B*). A decrease in UCP-1 transcript was also observed in the BAT of $AR^{L-/Y}$ mice (Fig. 5*C*), although it was less predominant than that in WAT; however, this is explained by the sevenfold higher expression of AR transcript in male WAT than BAT (Fig. 5*D*). The downregulation of UCP-1 might explain, to some extent, the lower V_{O_2} in

TABLE 2
Spontaneous activity at various life stages

Genotype	Body weight (g)	Distance (cm)	Speed composition			Rearing ∇ (n)	Rearing ∇ duration (s)
			% RT	% MS	% MF$^{\Delta}$		
8 weeks							
$AR^{X/Y}$	23 ± 0.69	98,816.3 ± 10,951.0	60.4	23.9	15.7	5,026.0 ± 1067.6	1.12 ± 0.23
$AR^{L-/Y}$	21 ± 1.34	66,394.8 ± 14,616.7*	72.8	17.8	9.48	2,410.5 ± 569.5*	1.20 ± 0.31
20 weeks							
$AR^{X/Y}$	31.90 ± 4.96	99,770.8 ± 27,281.6	65.8	20.9	13.3	7,003.2 ± 1575.7	1.14 ± 0.16
$AR^{L-/Y}$	41.07 ± 3.18*	60,608.8 ± 11,802.8*	72.9	19.7	7.5	3,188.5 ± 594.3*	1.06 ± 0.18
40 weeks							
$AR^{X/Y}$	35.46 ± 2.91	78,210.5 ± 23,996.3	67.4	21.4	11.2	3,497.7 ± 667.2	1.50 ± 0.24
$AR^{L-/Y}$	56.50 ± 7.83*	41,480.6 ± 7,164.4*	81.8	13.9	4.2	1,532.8 ± 409.5*	1.32 ± 0.43

*$P < 0.01$ compared with $AR^{X/Y}$ (wild-type controls), $n = 6$. ∇, rearing: mouse stands up on its hind legs. RT, resting: speed <2.00 cm/s; MS, moving slowly: speed between 2.00 and 5.00 cm/s; MF, moving fast: speed >5.00 cm/s.

$AR^{L-/Y}$ mice. In addition, another thermogenetic factor, PPAR-γ coactivator 1 (27), was also significantly decreased in both the WAT and BAT of $AR^{L-/Y}$ mice (Fig. 5*E* and *F*).

Hormone-sensitive lipase catalyzes the rate-limiting step of lipolysis in adipose tissue. The transcript level of hormone-sensitive lipase was significantly decreased in $AR^{L-/Y}$ WAT (Fig. 6*A*), whereas those for de novo lipid synthesis indicators, such as fatty acid synthase (Fig. 6*B*) and acetyl-CoA carboxylase (Fig. 6*C*) as well as the lipogenic transcriptional factor sterol regulatory element–binding protein-1c (Fig. 6*D*), were not significantly changed in both WAT and BAT (data not shown). Transcripts encoding lipoprotein lipase, the key enzyme involved in lipogenesis from circulating plasma triglyceride, were found significantly decreased in $AR^{L-/Y}$ WAT (Fig. 6*E*). The fatty acid β-oxidation markers carnitine palmitoyl transferase 1 (Fig. 6*F*) and long-chain acyl-CoA dehydrogenase (Fig. 6*G*) in $AR^{L-/Y}$ WAT showed lower trends, but they were not statistically significant. In total, decreased lipolysis rather than increased lipid synthesis might account for the increased adiposity in $AR^{L-/Y}$ mice.

DISCUSSION

Our AR null mice have neither detectable AR transcript nor protein, thus theoretically abolishing any effect of the androgens-AR system. Mirroring the increased fat mass observed in hypogonadal men, $AR^{L-/Y}$ mice have increased body weight, which is largely attributable to expanded adiposity, as indicated by both CT-based body composition analysis and anatomy. Body weights of ARKO female mice were unchanged (10), suggesting AR's effect on adiposity is specific to males. Dysfunction of the estrogen–estrogen receptor system was reported to be associated with obesity in male subjects based on the finding from both estrogen receptor-α–knockout (19) and aromatase knockout mice (20). Although we may be unable to completely exclude a possibly mixed effect on the $AR^{L-/Y}$ obese phenotype from the estrogen–estrogen receptor system, in which the function is theoretically impaired because of the shortage of the substrate for androgen-estrogen conversion in $AR^{L-/Y}$ mice, the possibility might be minor because we noticed that serum estrogen levels in $AR^{L-/Y}$ mice at both 8 weeks (12) and 40 weeks of age remain intact compared with $AR^{X/Y}$ mice, suggesting $AR^{L-/Y}$ mice are not in short supply of estrogen. In addition, supplementation of the nonaromatizable androgen dihydrotestosterone corrected fat mass increase in castrated $AR^{X/Y}$ mice but not in $AR^{L-/Y}$ mice (10), confirming that androgen actions mediated via AR has a distinct and independent adiposity-lowering effect in male subjects. Thus, our ARKO mice represent a powerful model for studying the role of the androgen-AR system in male adiposity regulation.

The direct molecular mechanism accounting for hypertrophic adipocytes and expanded WAT of $AR^{L-/Y}$ mice might rely on the altered lipid homeostasis characterized by decreased lipolysis but not increased lipogenesis. Transcripts for hormone-sensitive lipase are strikingly decreased, whereas those for lipogenetic genes (fatty acid synthase, acetyl-CoA carboxylase, sterol regulatory element–binding protein-1c, and lipoprotein lipase) are not increased (unchanged or decreased). The results are consistent with previous suggestions that androgens are lipolytic (28,29) and are very different from those of aromatase knockout mice, in which lipogenesis was found enhanced

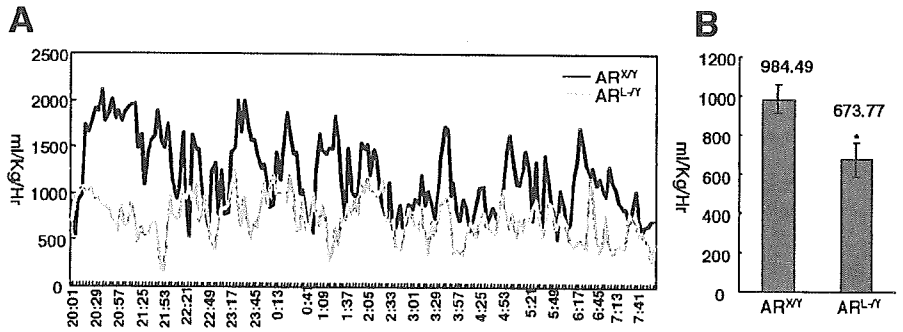

FIG. 4. Metabolic rate assessments in $AR^{L-/Y}$ and $AR^{X/Y}$ mice. *A*: Representative oxygen consumption (Vo_2) tracing curves (8 P.M. to 8 A.M.). *B*: Mean average Vo_2 values. *$P < 0.01$ compared with $AR^{X/Y}$ mice, $n = 6$.

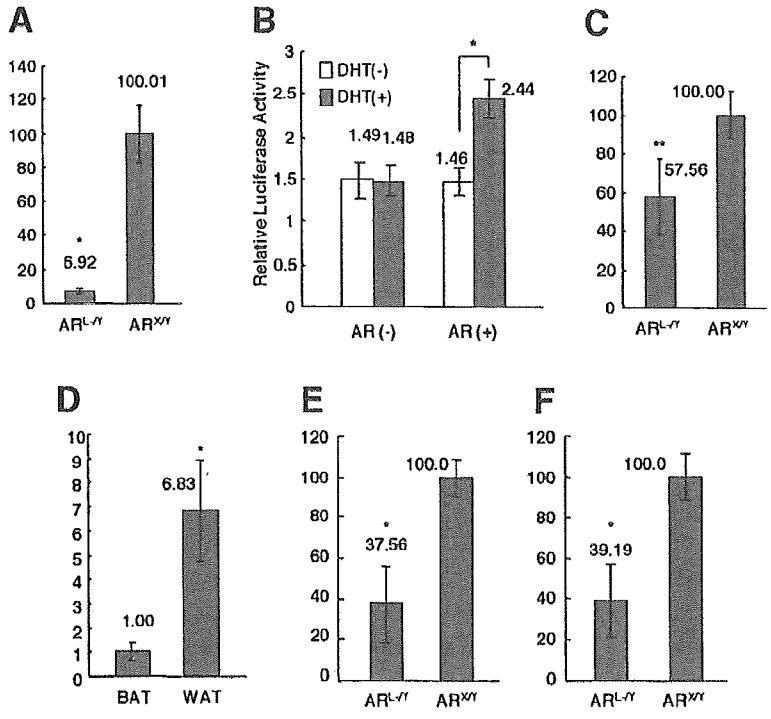

FIG. 5. Altered expressions of UCP-1. *A*: UCP-1 transcript levels in the WAT of $AR^{L-/Y}$ and $AR^{X/Y}$ mice. $AR^{X/Y}$ values were set at 100. *B*: Dual-luciferase assay of a 3.85-kb UCP-1 promoter in NIH-3T3-L1 adipocytes. In the absence of AR, dihydrotestosterone had no effect on UCP-1 promoter; however, the promoter was activated in a dihydrotestosterone-dependent manner in the presence of AR. *C*: UCP-1 transcript levels in the BAT of $AR^{L-/Y}$ and $AR^{X/Y}$ mice. $AR^{X/Y}$ values were set at 100. *D*: Relative AR transcript levels in BAT and WAT of $AR^{X/Y}$ mice. The AR transcript levels in BAT were set at 1.00. *E* and *F*: PPAR-γ coactivator 1 transcript levels in WAT (*E*) and BAT (*F*), respectively. $AR^{X/Y}$ values were set at 100. $^*P < 0.01$; $^{**}P < 0.05$ compared with $AR^{X/Y}$ mice or BAT (*D*) ($n = 6$). DHT, dihydrotestosterone.

(high lipoprotein lipase), but lipolysis was normal (30), suggesting estrogen is antilipogeneic.

Besides its negative role on adiposity, the androgen-AR system seems also to be negative to insulin sensitivity. Previous studies suggested androgen impairs insulin sensitivity in both humans and rodents (31,32). In our study, despite the obvious obese appearance, $AR^{L-/Y}$ mice reacted to both insulin and glucose challenges in manners that were indistinguishable from those of wild-type controls, indicating that the overall insulin sensitivity remained intact. This discordance between obesity and intact insulin-glucose homeostasis is unique to $AR^{L-/Y}$ mice, and it is very different from estrogen receptor-α knockout (19) or aromatase knockout (20) mice, which are accompanied by glucose intolerance and insulin resistance. One possible mechanism for the discordance might be hyperadiponectinemia. Adiponectin, originating from adipose tissue specifically, functions as an important insulin sensitizer (13,33) and correlates negatively with fat mass in that its plasma levels or adipose tissue mRNA levels decrease among obese subjects and recover after weight loss (34). The significant reduction of adiponectin transcripts in the WAT of obese $AR^{L-/Y}$ mice matches this conventional concept and thus suggests that downregula-

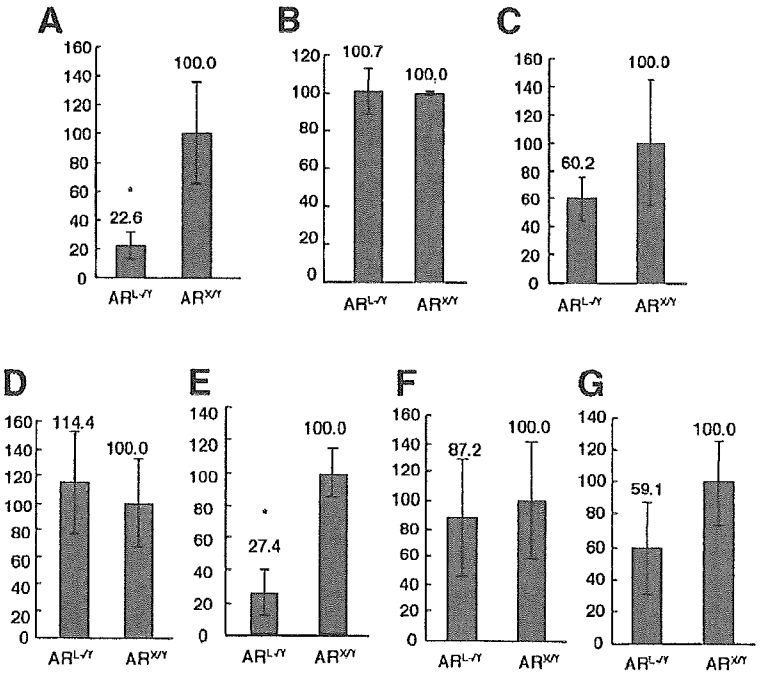

FIG. 6. WAT transcripts levels for genes involved in lipid homeostasis. *A*: Hormone-sensitive lipase transcript levels in WAT of $AR^{L-/Y}$ and $AR^{X/Y}$ mice. *B*: Fatty acid synthase transcript levels. *C*: Acetyl-CoA carboxylase transcript levels. *D*: Sterol regulatory element–binding protein 1c transcript levels. *E*: Lipoprotein lipase transcript levels. *F*: Carnitine palmitoyl transferase 1 transcript levels. *G*: Long-chain acyl-CoA dehydrogenase transcript levels. Transcripts levels in WAT of $AR^{X/Y}$ mice were set at 100. $^*P < 0.01$ compared with $AR^{X/Y}$ mice ($n = 6$).

tion happens at the transcriptional level. However, despite the lower mRNA level in WAT tissue, the serum protein level was surprisingly elevated, even after adjustment of WAT mass, indicating that the secretion process of adiponectin protein from WAT is relatively enhanced by AR inactivation. This supports a previous suggestion that testosterone inhibits adiponectin secretion from adipocytes (35,36). Thus, the androgen-AR system is an inhibitory player in the adiponectin secretion mechanism, which is largely unclarified. The inhibitory effect may also help explain the severe insulin resistance and hypoadiponectinemia observed in diseases with androgen excess, such as polycystic ovary syndrome, in which an AR blocker was found able to improve metabolic abnormalities and dysadipocytokinemia (37). Besides hyperadiponectinemia, the low expression of PPAR-γ in $AR^{L-/Y}$ WAT may also contribute to the unexpectedly normal insulin sensitivity because an intermediate level of PPAR-γ expression in WAT is the best condition for insulin sensitivity, as suggested by the finding that heterozygous PPAR-γ–deficient mice were protected from developing insulin resistance compared with wild-type mice (23).

The molecular events behind the intact glucose homeostasis, glucose uptake, and oxidation were found enhanced in skeletal muscle by AR inactivation, mirroring the clinical picture of polycystic ovary syndrome patients, where androgen excess is related with insulin resistance (32) and impaired glucose uptake (38). However, at this moment, we're not sure whether the enhanced glucose uptake and oxidation is caused directly by androgen-AR system inactivation or is secondary to hyperadiponectinemia or low PPAR-γ expression.

Body weight and the storage of energy as triglycerides in adipose tissue are homeostatically regulated by the long-term balance between energy intake and expenditure; obesity only develops if energy intake chronically exceeds the total energy expenditure (24). Although it doesn't affect appetite, AR inactivation causes an intrinsic decrease of spontaneous physical activity in male mice as well as overall oxygen consumption (V_{O_2}). Thus, androgen-AR system inactivation in male mice causes a chronic positive energy balance, which favors acceleration of fat mass and obesity.

In agreement with the lower V_{O_2}, both the thermogenic UCP-1 and PPAR-γ coactivator 1 transcripts were decreased in the adipose tissues of $AR^{L-/Y}$ mice. UCP-1, which uncouples energy substrate oxidation from mitochondrial ATP production and hence results in a loss of potential energy as heat, is one of the most important molecules responsible for adaptive thermogenesis (26). To our knowledge, this is the first time it has been shown that AR, upon its ligand binding, directly activates UCP-1 transcription, presumably by binding to the steroid response elements on the promoter.

Although AR directly regulates factors in the peripheral tissues involved in energy homeostasis, like UCP-1, it also very likely affects the mechanism exerted by the central nervous system because AR was found densely expressed in various hypothalamic nuclei, including the ventromedial hypothalamus and dorsomedial hypothalamus and the arcuate nucleus (39). The androgen-activating 5α-reductase is also expressed in the hypothalamus (40). The physiological role of the androgen-AR system in the hypothalamus is largely unknown. It is highly possible that the receptor may be involved in regulating the leptin-regulated melanocortin circuit because AR activation in the hypothalamus increases the inhibitory neuropeptide somatostatin (41,42), which may in turn inhibit the anorexigenic melanocyte-stimulating hormone or cocaine- and amphetamine-regulated transcript. The altered energy balance in $AR^{L-/Y}$ characterized by lower V_{O_2} and lower physical activity warrants further study of the intra–central nervous system role of AR, which is now ongoing.

In summary, the androgen-AR system is correlated with male adiposity, and inactivation of the system causes late-onset obesity in male mice because of altered energy balance, since the $AR^{L-/Y}$ mice were euphagic but less physically dynamic and less oxygen-consuming compared with $AR^{X/Y}$ mice. The mechanism of decreased energy expenditure might reside in both the central nervous system and peripheral tissues. Besides its negative role in adiposity, the androgen-AR system also plays a negative role in insulin sensitivity, at least in part through inhibiting the release of adiponectin from adipose tissue.

ACKNOWLEDGMENTS

This work was supported in part by a grant for the 21st Century COE Program from the Japanese Ministry of Education, Culture, Sports, Science, and Technology.

REFERENCES

1. Gustafson DR, Wen MJ, Koppanati BM: Androgen receptor gene repeats and indices of obesity in older adults. *Int J Obes Relat Metab Disord* 27:75–81, 2003
2. Jorgensen JO, Vahl N, Hansen TB, Fisker S, Hagen C, Christiansen JS: Influence of growth hormone and androgens on body composition in adults. *Horm Res* 45:94–98, 1996
3. Vermeulen A: Andropause. *Maturitas* 34:5–15, 2000
4. Kyle UG, Genton L, Hans D, Karesgard L, Slosman DO, Pichard C: Age-related differences in fat-free mass, skeletal muscle, body cell mass and fat mass between 19 and 94 years. *Eur J Clin Nutr* 55:663–672, 2001
5. Matsumoto AM: Andropause: clinical implications of the decline in serum testosterone levels with aging in men. *J Gerontol A Biol Sci Med Sci* 57:M76–M99, 2002
6. Katznelson L, Rosenthal DI, Rosol MS, Anderson EJ, Hayden DL, Schoenfeld DA, Klibanski A: Using quantitative CT to assess adipose distribution in adult men with acquired hypogonadism. *Am J Roentgenol* 170:423–427, 1998
7. Rolf C, von Eckardstein S, Koken U, Nieschlag E: Testosterone substitution of hypogonadal men prevents the age-dependent increases in body mass index, body fat and leptin seen in healthy ageing men: results of a cross-sectional study. *Eur J Endocr* 146:505–511, 2002
8. Wang C, Swedloff RS, Iranmanesh A, Dobs A, Snyder PJ, Cunningham G, Matsumoto AM, Weber T, Berman N: Transdermal testosterone gel improves sexual function, mood, muscle strength, and body composition parameters in hypogonadal men. *J Clin Endocrinol Metab* 85:2839–2853, 2000
9. Mauras N, Hayes V, Welch S, Rini A, Helgeson K, Dokler M, Veldhuis JD, Urban RJ: Testosterone deficiency in young men: marked alterations in whole body protein kinetics, strength, and adiposity. *J Clin Endocrinol Metab* 83:1886–1992, 1998
10. Sato T, Matsumoto T, Yamada T, Watanabe T, Kawano H, Kato S: Late onset of obesity in male androgen receptor-deficient (AR KO) mice. *Biochem Biophys Res Commun* 300:167–171, 2003
11. Sato T, Matsumoto T, Kawano H, Watanabe T, Uematsu Y, Sekine K, Fukuda T, Aihara K, Krust A, Yamada T, Kato S: Brain masculinization requires androgen receptor function. *Proc Natl Acad Sci U S A* 101:1673–1678, 2004
12. Kawano H, Sato T, Yamada T, Matsumoto T, Sekine K, Watanabe T, Nakamura T, Fukuda T, Yoshimura K, Yoshizawa T, Kato S: Suppressive function of androgen receptor in bone resorption. *Proc Natl Acad Sci U S A* 100:9416–9421, 2003

13. Maeda N, Shimomura I, Kishida K, Nishizawa H, Matsuda M, Nagaretani H, Furuyama N, Kondo H, Takahashi M, Arita Y, Komuro R, Ouchi N, Kihara S, Tochino Y, Okutomi K, Horie M, Takeda S, Aoyama T, Funahashi T, Matsuzawa Y: Diet-induced insulin resistance in mice lacking adiponectin/ACRP30. *Nat Med* 8:731–737, 2002
14. Fan W, Yanase T, Morinaga H, Mu YM, Nomura M, Okabe T, Goto K, Harada N, Nawata H: Activation of peroxisome proliferator-activated receptor-gamma and retinoid X receptor inhibits aromatase transcription via nuclear factor-kappaB. *Endocrinology* 146:85–92, 2005
15. Fan W, Yanase T, Wu Y, Kawate H, Saitoh M, Oba K, Nomura M, Okabe T, Goto K, Yanagisawa J, Kato S, Takayanagi R, Nawata H: Protein kinase A potentiates adrenal 4 binding protein/steroidogenic factor 1 transactivation by reintegrating the subcellular dynamic interactions of the nuclear receptor with its cofactors, general control nonderepressed-5/transformation/transcription domain-associated protein, and suppressor, dosage-sensitive sex reversal-1: a laser confocal imaging study in living KGN cells. *Mol Endocrinol* 18:127–141, 2004
16. Broulik PD, Schreiber V: Effect of alloxan diabetes on kidney growth in intact and castrated mice. *Acta Endocrinol* 99:109–111, 1982
17. Avdalovic N, Bates M: The influence of testosterone on the synthesis and degradation rate of various RNA species in the mouse kidney. *Biochim Biophys Acta* 407:299–307, 1975
18. Bachman ES, Dhillon H, Zhang CY, Cinti S, Bianco AC, Kobilka BK, Lowell BB: betaAR signaling required for diet-induced thermogenesis and obesity resistance. *Science* 297:843–845, 2002
19. Heine PA, Taylor JA, Iwamoto GA, Lubahn DB, Cooke PS: Increased adipose tissue in male and female estrogen receptor-alpha knockout mice. *Proc Natl Acad Sci U S A* 97:12729–12734, 2000
20. Jones ME, Thorburn AW, Britt KL, Hewitt KN, Wreford NG, Proietto J, Oz OK, Leury BJ, Robertson KM, Yao S, Simpson ER: Aromatase-deficient (ArKO) mice have a phenotype of increased adiposity. *Proc Natl Acad Sci U S A* 97:12735–12740, 2000
21. Simpson ER, Davis SR: Another role highlighted for estrogens in the male: sexual behavior. *Proc Natl Acad Sci U S A* 97:14038–14040, 2000
22. Combs TP, Berg AH, Philipp SB, Scherer E, Rossetti L: Endogenous glucose production is inhibited by the adipose-derived protein Acrp30. *J Clin Invest* 108:1875–1881, 2001
23. Kubota N, Terauchi Y, Miki H, Tamemoto H, Yamauchi T, Komeda K, Satoh S, Nakano R, Ishii C, Sugiyama T, Eto K, Tsubamoto Y, Okuno A, Murakami K, Sekihara H, Hasegawa G, Naito M, Toyoshima Y, Tanaka S, Shiota K, Kitamura T, Fujita T, Ezaki O, Aizawa S, Kadowaki T: PPAR gamma mediates high-fat diet-induced adipocyte hypertrophy and insulin resistance. *Mol Cell* 4:597–609, 1999
24. Spiegelman BM, Flier JS: Obesity and the regulation of energy balance. *Cell* 104:531–543, 2001
25. Lowell BB, Spiegelman BM: Towards a molecular understanding of adaptive thermogenesis. *Nature* 404:652–660, 2000
26. Argyropoulos G, Harper ME: Uncoupling proteins and thermoregulation. *J Appl Physiol* 92:2187–2198, 2002
27. Puigserver P, Spiegelman BM: Peroxisome proliferator-activated receptor-gamma coactivator 1 alpha (PGC-1 alpha): transcriptional coactivator and metabolic regulator. *Endocr Rev* 24:78–90, 2003
28. Xu X, De Pergola G, Bjorntorp P: The effects of androgens on the regulation of lipolysis in adipose precursor cells. *Endocrinology* 126:1229–1234, 1990
29. Sih R, Morley JE, Kaiser FE, Perry III HM, Patrick P, Ross C: Testosterone replacement in older hypogonadal men: a 12-month randomized controlled trial. *J Clin Endocrinol Metab* 82:1661–1667, 1997
30. Misso ML, Murata Y, Boon WC, Jones ME, Britt KL, Simpson ER: Cellular and molecular characterization of the adipose phenotype of the aromatase-deficient mouse. *Endocrinology* 144:1474–1480, 2003
31. Shoupe D, Lobo RA: The influence of androgens on insulin resistance. *Fertil Steril* 41:385–388, 1984
32. Toprak S, Yonem A, Cakir B, Guler S, Azal O, Ozata M, Corakci A: Insulin resistance in nonobese patients with polycystic ovary syndrome. *Horm Res* 55:65–70, 2001
33. Yamauchi T, Kamon J, Waki H, Imai Y, Shimozawa N, Hioki K, Uchida S, Ito Y, Takakuwa K, Matsui J: Globular adiponectin protected ob/ob mice from diabetes and ApoE-deficient mice from atherosclerosis. *J Biol Chem* 278:2461–2468, 2003
34. Pittas AG, Joseph NA, Greenberg AS: Adipocytokines and insulin resistance. *J Clin Endocrinol Metab* 89:447–452, 2004
35. Nishizawa H, Shimomura I, Kishida K, Maeda N, Kuriyama H, Nagaretani H, Matsuda M, Kondo H, Furuyama N, Kihara S, Nakamura T, Tochino Y, Funahashi T, Matsuzawa Y: Androgens decrease plasma adiponectin, an insulin-sensitizing adipocyte-derived protein. *Diabetes* 51:2734–2741, 2002
36. Lanfranco F, Zitzmann M, Simoni M, Nieschlag E: Serum adiponectin levels in hypogonadal males: influence of testosterone replacement therapy. *Clin Endocrinol (Oxf)* 60:500–507, 2004
37. Ibanez L, Valls C, Cabre S, De Zegher F: Flutamide-metformin plus ethinylestradiol-drospirenone for lipolysis and antiatherogenesis in young women with ovarian hyperandrogenism: the key role of early, low-dose flutamide. *J Clin Endocrinol Metab* 89:4716–4720, 2004
38. Holte J: Polycystic ovary syndrome and insulin resistance: thrifty genes struggling with over-feeding and sedentary life style? *J Endocrinol Invest* 21:589–601, 1998
39. Herbison AE: Neurochemical identity of neurones expressing oestrogen and androgen receptors in sheep hypothalamus. *J Reprod Fertil Suppl* 49:271–283, 1995
40. Poletti A, Martini L: Androgen-activating enzymes in the central nervous system. *J Steroid Biochem Mol Biol* 69:117–122, 1999
41. Zeitler P, Vician L, Chowen-Breed JA, Argente J, Tannenbaum GS, Clifton DK, Steiner RA: Regulation of somatostatin and growth hormone-releasing hormone gene expression in the rat brain. *Metabolism* 39:46–49, 1990
42. Hasegawa O, Sugihara H, Minami S, Wakabayashi I: Masculinization of growth hormone (GH) secretory pattern by dihydrotestosterone is associated with augmentation of hypothalamic somatostatin and GH-releasing hormone mRNA levels in ovariectomized adult rats. *Peptides* 13:475–481, 1992

ELSEVIER

EXPERIMENTAL HEMATOLOGY

Experimental Hematology 33 (2005) 857–864

Pivotal role of peroxisome proliferator–activated receptor γ (PPARγ) in regulation of erythroid progenitor cell proliferation and differentiation

Eriko Nagasawa[a], Yasunobu Abe[a], Junji Nishimura[b], Toshihiko Yanase[a], Hajime Nawata[a], and Koichiro Muta[a]

[a]*Department of Medicine and Bioregulatory Science, Graduate School of Medical Sciences, Kyushu University, Fukuoka, Japan;* [b]*Department of Clinical Immunology, Medical Institute of Bioregulation, Kyushu University, Beppu, Ohita, Japan*

(Received 30 November 2004; revised 7 April 2005; accepted 3 May 2005)

Objective. **The aim of this study was to reveal the role of peroxisome proliferator-activated receptor γ (PPARγ) in erythropoiesis.**

Methods. **The effects of PPARγ ligands on cellular proliferation and differentiation were investigated in erythroid colony-forming cells (ECFCs) purified from human peripheral blood.**

Results. **RT-PCR analysis revealed that PPARγ mRNA is expressed in ECFCs. Synthetic PPARγ ligands, troglitazone or pioglitazone, suppressed cellular proliferation without inducing apoptosis and delayed maturation of ECFCs, as determined by flow cytometry. The delay in erythroid maturation by troglitazone was confirmed by the down-regulation of γ-globin, β-globin and GATA-1 mRNA, and the maintenance of GATA-2 mRNA.**

Conclusions. **Our results suggest that PPARγ modulates the differentiation process of erythroid progenitor cells, and plays a crucial role in regulating the balance of hematopoiesis.**

Introduction

Peroxisome proliferator–activated receptor γ (PPARγ) is a ligand-activated transcriptional factor that belongs to the nuclear receptor superfamily [1]. It can be activated by 15-deoxy-$\Delta^{12,14}$-prostaglandin J_2 (15d-PGJ_2), a natural ligand for PPARγ [2,3], and thiazolidinediones (TZDs), which are chemically synthesized PPARγ ligands used to treat insulin-resistant patients with type 2 diabetes mellitus [4]. It has been reported that PPARγ is expressed at high levels in adipose tissue and that it plays an essential role in adipocyte differentiation [5,6]. However, PPARγ has also been detected in many other cell lines, including hepatocytes, fibroblasts, and breast and colon epithelial cells [7].

With regard to hematopoietic tissues, PPARγ is reportedly expressed in bone marrow stromal cells, $CD34^+$ progenitor cells, normal monocytes/macrophages, lymphocytes, and neutrophils [8,9]. PPARγ ligands have been shown to modulate proliferation and differentiation of various human leukemic cell lines [10–13]. Furthermore, administration of TZDs resulted in impaired erythropoiesis, as well as fat accumulation in the bone marrow cavity in both rodent and canine models [14–16]. Replacement of hematopoeitic tissue with fatty marrow is a characteristic feature of aplastic anemia. Indeed, slight anemia is known to be a possible side effect of TZDs in patients with diabetes mellitus [17]. This evidence suggests that PPARγ plays crucial role in erythropoiesis, as well as in adipogenesis.

In the present study, we showed that PPARγ ligands modulate proliferation and maturation of erythroid progenitor cells.

Materials and methods

Reagents

Recombinant human erythropoietin (rhEPO) was kindly provided by Chugai Pharmaceutical Co., Ltd. (Tokyo, Japan); recombinant human interleukin-3 (rhIL-3), and recombinant human stem cell factor (rhSCF) were kindly provided by Kirin Brewery Co., Ltd. (Tokyo, Japan). Troglitazone and pioglitazone were kindly provided by Sankyo Chemical Industries and Takeda Chemical Industries (Tokyo, Japan), respectively, while 15d-PGJ_2 was purchased from BIOMOL (Plymouth Meeting, PA, USA). The irreversible PPARγ antagonist GW9662 was purchased from Cayman Chemical

Offprint requests to: Koichiro Muta, M.D., Department of Medicine and Bioregulatory Science, Graduate School of Medical Sciences, Kyushu University, 3-1-1 Maidashi, Higashi-ku, Fukuoka 812-8582, Japan; E-mail: mmmmm@intmed3.med.kyushu-u.ac.jp

0301-472X/05 $–see front matter.
doi: 10.1016/j.exphem.2005.05.003

(Ann Arbor, MI, USA). These compounds were dissolved in dimethylsulfoxide (DMSO) containing 10% bovine serum albumin (BSA; Stem Cell Technologies, Vancouver, BC, Canada), and final concentrations of DMSO and BSA were 0.1% or less.

Purification and expansion of ECFCs

Erythoid colony-forming cells (ECFCs) were prepared as previously described [18–22]. Light-density mononuclear cells were obtained from peripheral blood buffy coats from normal, healthy Japanese volunteers, using density centrifugation. Adherent cells were depleted via 1-hour incubation in a polystyrene tissue-culture flask at 4°C. Nonadherent cells were then collected and 2 cycles of negative selection were performed using anti-CD3, -CD11b, -CD15, and -CD45RA antibodies and immunomagnetic beads with Vario-Macs columns (Miltenyi Biotech, Auburn, CA, USA). The remaining cells were cultured in Iscove's modified Dulbecco medium (IMDM; GIBCO BRL, Grand Island, NY, USA) containing 15% heat-inactivated fetal calf serum (FCS; Commonwealth Serum Laboratories, Melbourne, Australia), 15% pooled human AB serum, 2 U/mL rhEPO, 20 ng/mL rhSCF, 10 ng/mL rhIL-3, 100 U/mL penicillin, and 100 μg/mL streptomycin (GIBCO) at 37°C in 5% CO_2/95% air in a high-humidity incubator (day 0). On day 3, the cells, referred to as day-3 ECFCs, were centrifuged over lymphocyte separation medium (LSM), then collected and incubated under the same conditions, but in the absence of IL-3, and in the presence or absence of various PPARγ agonists. These cells were then used in the subsequent experiments. In some experiments, day-3 ECFCs were pretreated with the irreversible antagonist GW9662 [23] for 30 minutes before the PPARγ agonists were added.

Immunocytochemistry

Cells were cytospun onto glass slides and fixed with 2.5% formaldehyde. The cells were permeabilized in phosphate-buffered saline (PBS)-Igepal CA-630 (Sigma, St. Louis, MO, USA) for 15 minutes. Endogenous peroxidase activity was quenched with 0.3% H_2O_2, nonspecific binding was blocked with 10% normal rabbit serum (Nichirei, Tokyo, Japan). Slides were then incubated overnight with mouse monoclonal IgG_1 anti- PPARγ antibody (E-8, Santa Cruz Biotechnology, Santa Cruz, CA, USA) or mouse monoclonal IgG_1 anti-CD71 antibody (DF1513, Santa Cruz) or isotype control mouse IgG_1 antibody (Chemicon Europe, Hampshire, UK) at 10 μg/mL. After rinsing with PBS, cells were treated with a biotin-labeled goat anti-mouse IgG secondary antibody (Nichirei) for 1 hour, followed by peroxidase-conjugated streptavidin (Nichirei) for 30 minutes. Slides were developed with diaminobenzidine reagent, counterstained with methyl green, and visualized with an Olympus BX51 microscope (Olympus, Tokyo, Japan).

Determination of cell viability and apoptosis

Viability of cells was determined by trypan blue exclusion using a hemocytometer. Apoptosis was measured by flow cytometry using annexin V and propidium iodide (PI) as previously described [21,22].

MTT colorimetric assay

Cell growth was examined using the MTT colorimetric assay (Chemicon International, Osaka, Japan). Day-8 ECFCs were washed with IMDM and plated into serum-free liquid medium containing 50% IMDM/50% F-12 medium (Sigma Chemical, St. Louis, MO, USA) with 1% BSA, 300 μg/mL iron-saturated transferrin (652202, Boehringer Mannheim, Germany) lipid suspension prepared as described elsewhere [21,22], and 10 U/mL rhEPO in 96-well tissue culture plates. MTT solution (1 mg/mL) was added to each well, and cells were further incubated for 4 hours at 37°C. Absorbance at a wavelength of 570 nm was measured by a micro-ELISA reader.

Measurement of DNA synthesis

DNA synthesis was examined using a quantitative ELISA kit (Cell Proliferation ELISA; Roche, Diagnostics GmbH, Mannheim, Germany) that measures bromodeoxyuridine (BrdU) incorporation. The assay was performed according to the manufacturer's instructions. Briefly, day-7 ECFCs were labeled with BrdU for 2 hours. Cells were then fixed and incubated with anti-BrdU-peroxidase for 1 hour at room temperature. Absorbance was measured at 450 nm using a micro-ELISA reader.

Cell-cycle analysis

Cell cycle profiles were determined by flow cytometry [11]. Day-7 ECFCs were washed once in PBS and were then fixed on ice with 1% paraformaldehyde in PBS for 15 minutes. After cells were washed again with PBS, they were stored at −20°C with 70% ethanol for at least 4 hours. Finally, after treatment with 150 μg/mL RNase A, staining of cell nuclei was performed using 15 μg/mL PI for 15 minutes at 4°C. DNA contents were analyzed by flow cytometry using a FACScan (Becton-Dickinson, San Jose, CA, USA). The percentage of cells in the G0/G1, S, and G2/M phases of the cell cycle was determined using ModFIT software (Verity Software House, Topsham, ME, USA).

Assessment of cell differentiation by flow cytometry

The expression of transferrin receptor (TfR) and glycophorin A (GPA) on ECFCs was analyzed by flow cytometry, as described elsewhere [22]. Cells (1×10^5) were washed twice with PBS and were then incubated with fluorescein isothiocyanate (FITC)-conjugated anti-glycophorin A MoAb (11E4B-7-6, IM2212; Immunotech, Marseilles, France) and phycoerythrin (PE)-conjugated anti-CD71 MoAb (YDJ1.2.2, IM2001; Immunotech) for 30 minutes on ice. Samples were analyzed using the Epics Elite ESP flow cytometer (Coulter, Miami, FL, USA).

Determination of benzidine positivity

Aliquots of the cultures were cytocentrifuged onto glass slides, and the slides were stained with 3,3'-dimethoxybenzidine-hematoxylin and May-Grünwald-Giemsa [20]. The percentage of benzidine-positive cells was determined by counting 200 cells.

Plasma clot assay

The erythroid colony-forming capacity of ECFCs was determined using the plasma clot method [19–22]. After 7 days of liquid culture of day-3 ECFCs, adjusted number of day-10 cells (600 cells) in media consisting of IMDM, 20% FCS, 1% BSA, 10 ng/mL rhSCF, 2 U/mL rhEPO, and 10% citrated human AB plasma were plated in triplicate 35-mm culture dishes and incubated for a further 7 days. Clots were then fixed and stained with 3,3'-dimethoxybenzidine. Colonies of 8 or more hemoglobinized cells were defined as colony-forming unit-erythroid (CFU-E), and aggregates consisting of 2 to 7 hemoglobinized cells were defined as small erythroid clusters. Colonies consisting of 8 to 19 hemoglobinized cells were referred as to medium erythroid colonies, and those consisting of 20 to 49 hemoglobinized cells were referred to as large erythroid colonies [21].

Table 1. Primer and fluorogenic probe sequences for real-time RT-PCR assays

Gene	Primer/probe sequence	Size (bp)
γ-globin		219
primer	5′-GGCAACCTGTCCTCTGCCTC-3′	
	5′-GAAATGGATTGCCAAAACGG-3′	
β-globin		288
primer	5′-AGGTTCTTTGAGTCCTTTG-3′	
	5′-AGCCACCACTTTCTGATAG-3′	
GATA-1		378
primer	5′-TCAATTCAGCAGCCTATTCC-3′	
	5′-TTCGAGTCTGAATACCATCC-3′	
GATA-2		279
primer	5′-TGTTGTGCAAATTGTCAGACG-3′	
	5′-CATAGGTGCCATGTGTCCAGC-3′	
β-actin		460
primer	5′-CCAACCGCGAGAAGATGAC-3′	
	5′-GGAAGGAAGGCTGGAAGAGT-3′	
probe	LC-Red-5′-GGACCTGGCTGGCCGGGACCTGA-3′	
	5′-CCTCCCCCATGCCATCCTGCGTC-FITC	

Reverse-transcriptase polymerase chain reaction (RT-PCR) and real-time quantitative RT-PCR

Total RNA was isolated from 10^6 cells with TRIzol reagent (Invitrogen Corp., Carlsbad, CA, USA). First-strand cDNA was synthesized from 1 μg of total RNA using an RT-PCR kit (Takara, Shiga, Japan). Based on the human PPARγ2 sequence [6], 276 bp of the DNA sequence was amplified by PCR using sense and antisense primers (5′-ACAGAGATGCCATTCTGGCCC3′ and 5′CTTATTGTAGAGCTGAGTCTTCTC-3′, respectively). These primers were designed to amplify a region common to both PPARγ1 and γ2. As a control, a 242-bp β-actin cDNA sequence was amplified using sense and antisense primers (5′-TCGTGCGTGACATTAAGGAG3′ and 5′-GATGTCCACGTCACACTTCA-3′, respectively). The PCR reactions for PPARγ and β-actin cDNAs were performed with 30 amplification cycles (denaturation at 94°C for 1 minute, annealing at 53°C for 2 minutes, and extension at 72°C for 3 minutes) [12]. PCR products were visualized with ethidium bromide on 2% agarose gels. We verified the nucleotide sequence of each PCR product by direct sequencing [24] using the appropriate primers.

Quantitative real-time PCR assay of transcripts was carried out using gene-specific double fluorescent-labeled probes and LightCycler Software Version 3.5 (Roche, Diagnostics GmbH, Mannheim, Germany). The sequences of primers and probes used for real-time RT-PCR analysis are listed in Table 1 [25–27]. Target quantities were normalized against β-actin RNA and were calibrated using day-3 values, which were given a value of 1.0. All quantities were expressed as n-fold relative to the calibrator (day 3).

Statistical analysis

Student's *t*-test was used to determine significant differences between the groups and results are expressed as mean ± SD.

Results

Expression of PPARγ in ECFCs

The expression of PPARγ in ECFCs was first examined by RT-PCR. PPARγ is expressed in day-3 and day-7 ECFCs, but not in day-0 ECFCs (Fig. 1).

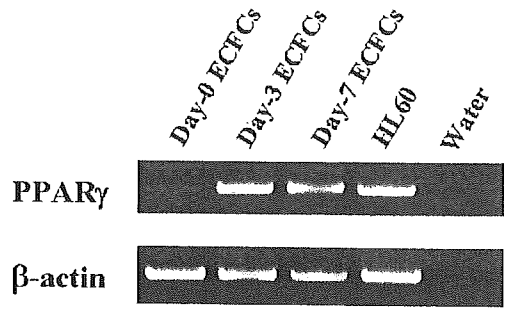

Figure 1. ECFCs expressed PPARγ mRNA. RT-PCR analysis of ECFCs was performed at the indicated times during erythroid maturation in liquid culture (details in Material and methods). The HL60 cell line was also examined as a positive control. Expression of the housekeeping gene β-actin was used as an internal control. PCR products were electrophoresed on 2% agarose gels and were visualized by ethidium bromide staining.

The presence of PPARγ in day-3 and day-7 ECFCs was further examined by immunocytochemistry. The purity of day-3 ECFCs, with burst-forming unit-erythroid (BFU-E)-like features, was 63.0% ± 7.8%, as determined in cytospin preparations. They had slightly ovoid cytoplasm with fine nuclear chromatin structure, basophilic cytoplasm, and multiple nucleoli (Fig. 2A). This percentage of erythroid cells was confirmed by immunocytochemistry (Fig. 2D) and flow cytometric analysis (data not shown) for the erythroid marker TfR. The remaining ~38% of day-3 cells were nonerythroid cells, which exhibit features such as those of lymphocytes, neutrophils, monocytes, and macrophages (Fig. 2A). In day-3 cells, erythroid cells expressed PPARγ protein, although the staining intensity was weaker than that of macrophages. The PPARγ staining pattern of ECFCs was cytoplasmic, as well as nuclear (Fig. 2C). At day 7, approximately 95% of the cells showed basophilic erythroblast features (Fig. 2E), and they were positive for TfR (Fig. 2H). These cells were also positive for PPARγ protein and the staining was in the cytoplasm and the nucleolus (Fig. 2G), but the PPARγ staining intensity was weaker when compared with day-3 ECFCs. The results were confirmed by real-time quantitative PCR analysis (data not shown).

Troglitazone delayed cellular proliferation of ECFCs without inducing apoptosis

In order to determine the effects of PPARγ ligands on proliferation of ECFCs, day-3 ECFCs were incubated with a synthetic PPARγ ligand, troglitazone. Addition of troglitazone to the liquid culture reduced the number of ECFCs in a dose-dependent manner (Fig. 3A). Significant reductions in cell number were observed from day 6 at 10 μM troglitazone ($p < 0.05$, as compared to control), and the maximum effect of troglitazone was observed at day 8 ($p < 0.005$, at 10 μM). When cellular growth was assessed by MTT assay (Fig. 3B), significant suppression was observed at 20 μM troglitazone ($p < 0.001$, at day 8). Trypan blue exclusion tests showed that the viability of ECFCs was not affected by

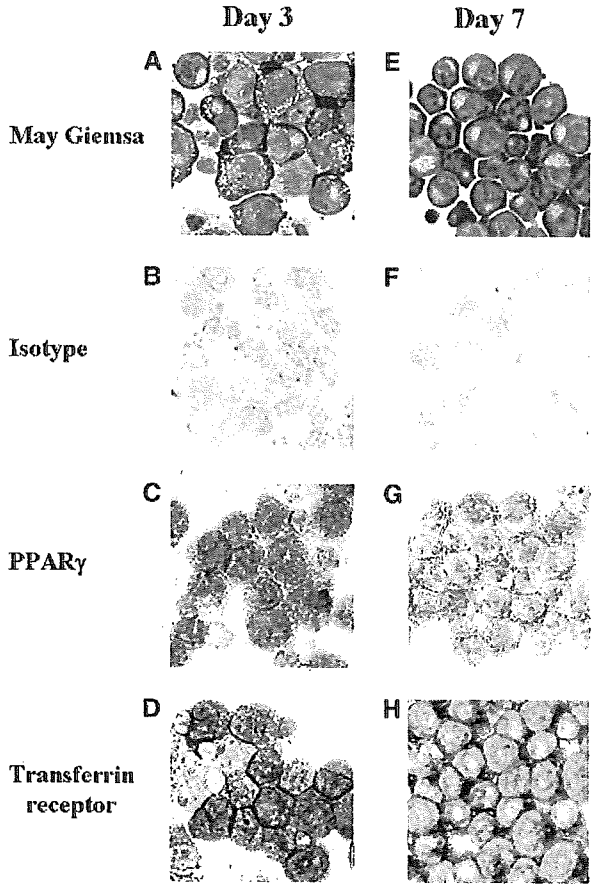

Figure 2. Immunocytochemistry demonstrating PPARγ protein expression in ECFCs. **(A–D)**: Day-3 ECFCs; **(E–H)**; day-7 ECFCs. Morphological changes in ECFCs were examined by May-Giemsa staining **(A,E)**. Immunocytochemistry was performed with a mouse monoclonal anti-PPARγ antibody **(C,G)** or a mouse monoclonal anti-TfR antibody **(D,H)** as described in Materials and methods. Nonspecific staining was assessed using a mouse IgG_1 isotype control **(B,F)**. Original magnification is ×1000. Pictures shown are representative of 4 experiments.

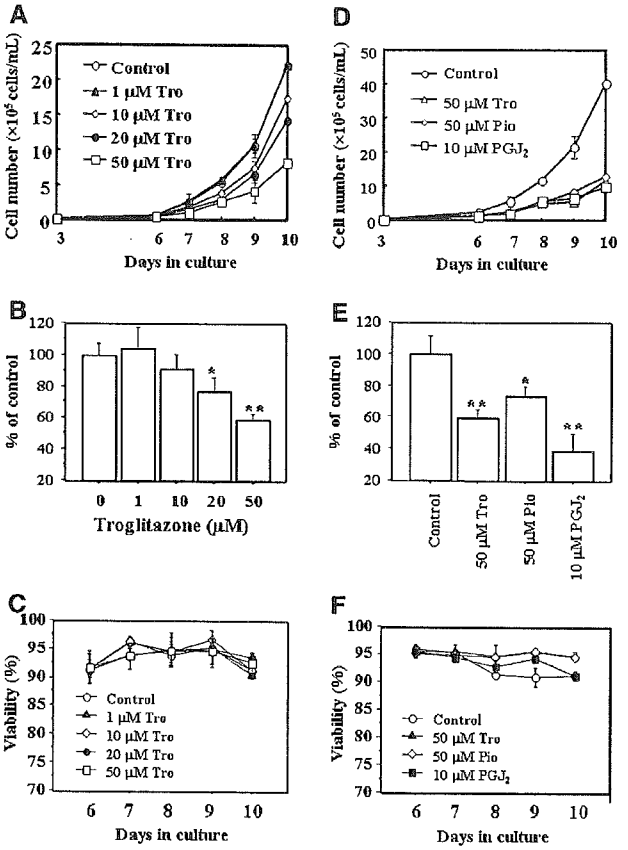

Figure 3. PPARγ ligands suppressed cellular proliferation of ECFCs without inducing apoptosis. **(A)**: Changes in viable number of ECFCs in the presence of different concentrations of troglitazone were determined by trypan blue exclusion. Troglitazone was added to the liquid culture on day 3. **(B)**: Cell growth was measured by MTT assay. Day-3 ECFCs were incubated for 5 days with various concentrations of troglitazone. On day 8, cells were transferred to serum-free medium and were incubated for 4 hours with MTT solution. Data are graphed as a percentage relative to DMSO controls. Data are the mean ± SD of 6 experiments. $^{*}p < 0.001$. $^{**}p < 0.0001$ as compared to controls (without troglitazone). **(C)**: Viability of ECFCs with different concentrations of troglitazone was evaluated by trypan blue exclusion. Each point indicates the mean ± SD of 2 experiments (each in duplicate). **(D–F)**: Day-3 ECFCs were incubated with troglitazone (50 μM), pioglitazone (50 μM), and 15d-PGJ_2 (10 μM). The total number of viable cells **(D)** and viability **(F)** were determined by trypan blue exclusion every day from day 6 to day 10, and MTT assay **(E)** was performed at day 8. Results are shown as mean ± SD of triplicate cultures. $^{*}p < 0.05$. $^{**}p < 0.01$ as compared to controls.

addition of troglitazone (Fig. 3C). Although apoptosis was measured by flow cytometry, there was no significant difference between untreated cells and troglitazone-treated cells (data not shown). When other TZD, pioglitazone and a natural PPARγ ligand, 15d-PGJ_2, were tested, proliferation of ECFCs was suppressed without affecting cell viability, as was seen with troglitazone (Fig. 3D–F).

In order to investigate the effects of PPARγ ligands on DNA synthesis of ECFCs, BrdU ELISA was performed. As shown in Figure 4, treatment with PPARγ ligands led to a decrease in the amount of BrdU incorporation into DNA. We next investigated the possible effects of troglitazone on cell-cycle distribution of ECFCs by FACS analysis. When ECFCs were exposed to 50 μM troglitazone, the proportion of cells in S phase decreased, but the effect was very weak (Fig. 4).

Interestingly, the ECFCs cultured with troglitazone seemed to continue proliferating after day 12, when the number of ECFCs cultured without troglitazone had reached plateau. To clarify whether PPARγ ligand delays or inhibits ECFC proliferation, we cultured ECFCs for a total of 17 days under three sets of conditions: no troglitazone added (control group), troglitazone added on day 3 and washed out on day 10 (wash-out group), and troglitazone added on day 3 and washed out on day 10 and added again immediately after wash-out (troglitazone group). Although cell number in the control group reached plateau at day 12, that of the wash-out group had caught up and exceeded that of the control

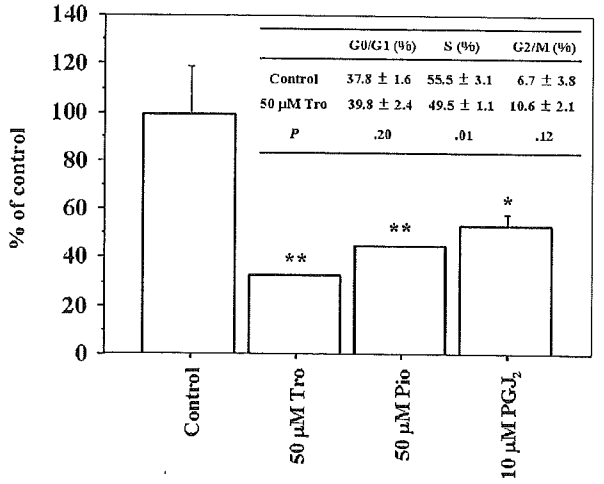

Figure 4. Effects of PPARγ ligands on DNA synthesis and cell cycle of ECFCs. Day-3 ECFCs were incubated with troglitazone (50 μM), pioglitazone (50 μM), and 15d-PGJ_2 (10 μM). DNA synthesis was quantified by BrdU incorporation at day 7. Results are expressed as a percentage relative to untreated samples. Values are mean ± SD of 6 replicates. $^{*}p < 0.05$. $^{**}p < 0.01$ as compared to control. Cell-cycle distribution was determined by FACS analysis after staining with PI at day 7. Results are presented as a percentage of the total cell population. Values are mean ± SD of four individual experiments.

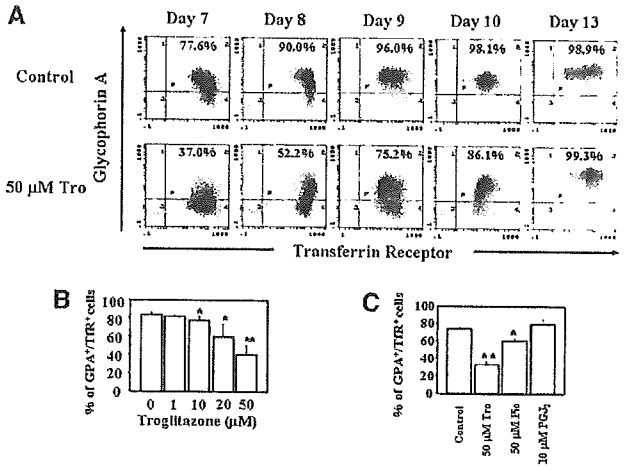

Figure 6. Troglitazone suppressed expression of glycophorin A on ECFCs. (A): Expression of GPA and TfR on ECFCs was determined by flow cytometry at the indicated times during erythroid maturation in liquid culture with 15% FCS, 15% human AB serum, 20 ng/mL rhSCF, and 2 U/mL rhEPO in the presence or absence of troglitazone (50 μM). Troglitazone was added to the liquid culture at day 3. Data are representative of 5 independent experiments. (B): Evaluation of the effects of 1–50 μM troglitazone on GPA/TfR expression in ECFCs at day 8 by flow cytometry. Each value indicates the mean ± SD of 2 experiments (each in duplicate). $^{*}p < 0.05$. $^{**}p < 0.01$ as compared to cultures without troglitazone. (C): Evaluation of the effects of various PPARγ ligands, troglitazone (50 μM), pioglitazone (50 μM), and 15d-PGJ_2 (10 μM), on GPA/TfR expression in ECFCs at day 8 by flow cytometry. Each value indicates the mean ± SD of triplicate dishes. $^{*}p < 0.005$. $^{**}p < 0.0001$ as compared to controls.

group at day 14, while that of the troglitazone group continued to increase until day 17 (Fig. 5).

Troglitazone delayed maturation of ECFCs

In liquid culture, ECFCs undergo terminal erythroid maturation, as characterized by drastic changes in the expression of GPA and TfR [22]. To determine the effects of troglitazone on maturation of ECFCs, expression of GPA and TfR was analyzed by flow cytometry. When troglitazone was added to the cultures, the expression of GPA was significantly reduced in a dose-dependent manner (Fig. 6A,B). These results indicate that addition of troglitazone to the culture delays erythroid maturation of ECFCs. The other TZD, pioglitazone (50 μM), also decreased GPA expression in ECFCs (no additives, 73.8% ± 2.2%; pioglitazone, 60.2% ± 2.8%, $p = 0.0028$), although the decrease was less substantial than that seen with troglitazone (33.2% ± 3.8%, $p < 0.0001$), while the natural PPARγ ligand 15d-PGJ_2 (10 μM) did not exhibit a significant effect (79.4% ± 6.0%, $p = 0.21$) (Fig. 6C). Although the effects of the specific PPARγ antagonist GW9662 were tested, evaluable data was not obtained due to its toxicity (data not shown).

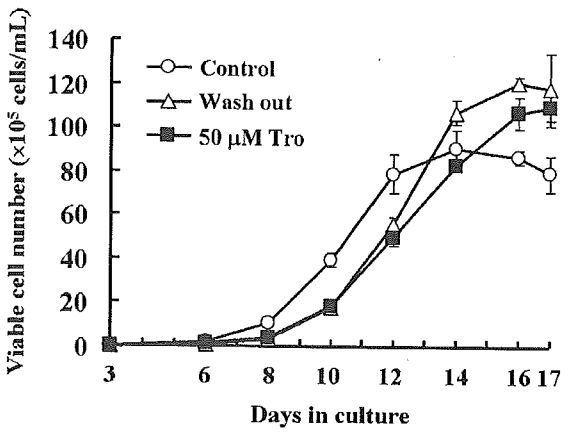

Figure 5. Troglitazone delayed cellular proliferation of ECFCs. ECFCs were cultured for a total of 17 days under three sets of conditions: no troglitazone added (control group), troglitazone added on day 3 and washed out on day 10 (wash-out group), troglitazone added on day 3, washed out on day 10, and added again immediately after wash-out (troglitazone group).

This delay in erythroid maturation by treatment with troglitazone was also evident in cytospin preparations stained with benzidine. When ECFCs were cultured with troglitazone, day-12 cells retained immature features and the intensity of benzidine staining was weak, while ECFCs cultured without troglitazone exhibited normal terminal erythroid maturation with nuclear condensation and enucleation, and were stained strongly with benzidine (Fig. 7A). When the percentage of benzidine-positive cells was determined serially, that of troglitazone cultures was significantly smaller than that seen in control cultures (Fig. 7B).

In order to determine whether troglitazone maintains the proliferative capacity of ECFCs during liquid culture, plasma-clot assays were performed. After liquid culture for

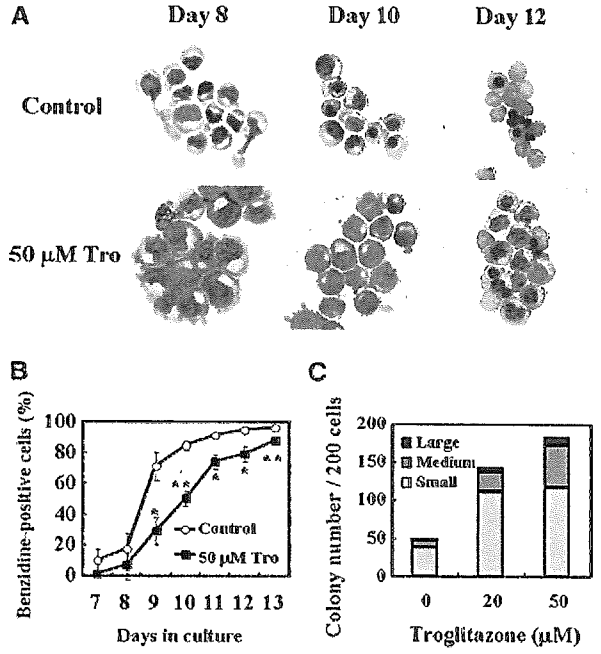

Figure 7. Troglitazone delayed maturation of ECFCs. ECFCs were incubated in liquid culture with 15% FCS, 15% human AB serum, 20 ng/mL rhSCF, and 2 U/mL rhEPO in the presence or absence of troglitazone (50 μM). (**A**): Morphological findings of ECFCs stained with benzidine and May-Giemsa at the indicated times (original magnification, ×1000). (**B**): Evaluation of the effects of troglitazone (50 μM) on benzidine positivity in ECFCs. The percentage of benzidine-positive cells was determined by counting 200 cells. Data are mean ± SD of triplicates. $^{*}p < 0.01$. $^{**}p < 0.001$ as compared to controls. (**C**): Erythroid colony-forming capacity after liquid culture for 7 days with or without troglitazone (20 μM, 50 μM) was determined by plasma clot assay. After 7 days of liquid culture of day-3 ECFCs, an adjusted number of day-10 cells were transferred to plasma-clot cultures (200 cells/well) and incubations were carried out for a further 7 days. The number of colonies was measured after benzidine staining. Large erythroid colonies include more than 20 hemoglobinized cells per colony; medium erythoid colonies include 8 to 19 cells per colony; and small erythroid clusters include 2 to 7 hemoglobinized cells per aggregate. Each point indicates the mean of triplicates.

7 days, with or without troglitazone, equal numbers of day-10 ECFCs were transferred to plasma-clot cultures and incubations were carried out for a further 7 days. The total number of clusters and colonies and the number of large- and medium-sized colonies formed from cells incubated with troglitazone were greater than those seen in cultures without troglitazone (Fig. 7C). These results indicate that addition of troglitazone results in maintenance of a greater colony-forming capacity than that seen without troglitazone, probably as a result of delayed cellular maturation.

Effects of troglitazone on expression of transcription factors involved in erythroid differentiation

In order to examine the mechanism by which troglitazone delays erythroid maturation, we compared the expression levels of two other transcription factors that are known to be involved in the development of erythroid cells using real time RT-PCR. When troglitazone (50 μM) was added to the liquid culture, the expression levels of γ-globin, β-globin, and GATA-1 were significantly downregulated, whereas expression of GATA-2 mRNA was sustained (Fig. 8).

Discussion

We previously showed that the synthetic PPARγ ligands TZDs induce suppression of both cell proliferation and expression of the erythroid marker GPA in the erythroleukemia cell line K562 [12]. Therefore, we hypothesized that the anemia observed in patients treated with TZDs may be explained by the suppression of erythropoiesis. In the present study, we demonstrated that TZDs delayed the maturation and proliferation of primary erythroid progenitor cells. These observations strongly support the above hypothesis.

Immunocytochemistry showed that both erythroid and nonerythroid cells possess PPARγ protein. This raises the question of whether nonerythroid cells contaminating the cultures secrete cytokines in response to PPARγ ligands. To answer this question, we performed positive selection of $CD71^{+}$ erythroid progenitors using anti-CD71 antibodies and immunomagnetic beads at day 3, and cultured with or without troglitazone. The effects of troglitazone, which delays proliferation and maturation of erythroid cells, were preserved in the absence of nonerythroid cells (data not shown).

In addition to TZDs, the natural PPARγ ligand 15d-PGJ_2 suppressed cellular proliferation of ECFCs, thus suggesting that these antiproliferative effects are mediated by

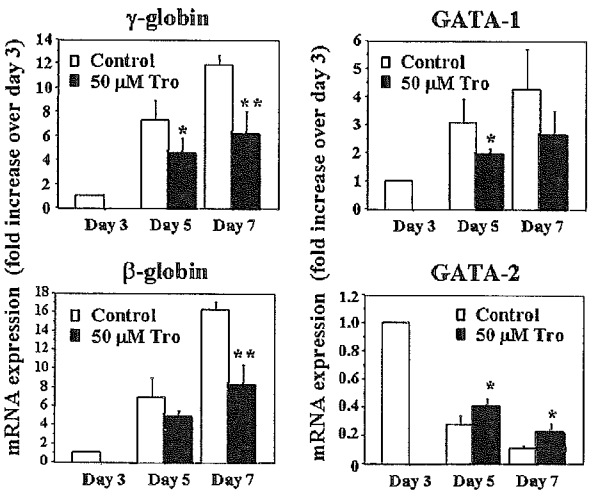

Figure 8. Effects of troglitazone on expression of genes involved in erythroid differentiation. Day-3 ECFCs were incubated with or without troglitazone (50 μM), and expression of γ-globin, β-globin, GATA-1, and GATA-2 mRNA was then quantified by real-time RT-PCR at the indicated times. Gene expression was normalized against an internal control, β-actin, and data are presented as fold change compared with day-3 ECFCs. Data are mean ± SD of three independent experiments. $^{*}p < 0.05$. $^{**}p < 0.005$ as compared to controls.

PPARγ. Although it has been reported that PPARγ ligands suppress cell growth by inducing apoptosis in various human leukemic and lymphoma cell lines [10–13,28–30], in this study, PPARγ ligands suppressed cell proliferation without reducing viability and enhancing apoptosis in ECFCs. These observations suggest that the reduction in cell number is due to inhibition of ECFC proliferation, rather than via apoptotic cell death. As shown in Figure 4, troglitazone treatment decreased DNA synthesis markedly in the BrdU experiment, but it only very slightly reduced the proportion of cells in S phase in the PI experiment. There is substantial disparity in the results of the BrdU and PI experiments. The BrdU experiment measures BrdU incorporation into the DNA of proliferating cells, thus measuring the amount of DNA synthesis. On the other hand, the PI experiment indicates the proportion of cells in the S phase of cell cycle. Troglitazone appears to delay the cell cycle rather than inducing cell-cycle arrest. Therefore, the percentage of cells in each phase may not have been affected by troglitazone treatment. Similar results were observed in SCF stimulation. Sakatoku et al. [31] showed that the proportion of cells in the S and G2 + M phases did not significantly differ following treatment with SCF in combination with EPO and EPO alone, but the absolute cell counts in the S and G2 + M phases were significantly higher with EPO + SCF stimulation than with EPO alone.

In this culture system, it has been reported that the proliferative capacity of ECFCs is closely linked with the state of cellular maturation [18]. In the early period of this liquid culture (days 3–6), BFU-E-like progenitors proliferate relatively slowly. During the intermediate period (days 7–11), CFU-E-like progenitors reach maximum proliferative capacity, and subsequently lose this capacity at later stages of maturation (days 12–14). Here, we showed that the number of troglitazone-treated cells caught up with that of cells cultured without troglitazone by day 14. This observation suggests that PPARγ ligands suppress proliferation of ECFCs by delaying the peak in proliferative capacity and preserving the immature stage. We previously reported that SCF delays maturation while stimulating ECFC proliferation by expanding the progenitor cell pool that is capable of producing a large number of erythrocytes [20]. The differences between our results and those obtained with SCF might be due to differences in the signal pathways that delay maturation of ECFCs, or an additional direct stimulatory effect of SCF on proliferation that overcomes the delay in maturation.

We revealed that the delay in erythroid maturation by troglitazone is accompanied by downregulation of γ-globin, β-globin, and GATA-1 mRNA and maintenance of GATA-2 mRNA. In models of hemoglobin biosynthesis in adults, a transition from fetal (γ-globin; HbF) to adult (β-globin; HbA) types has been demonstrated during the differentiation process [32]. Phenylbutyrate and its related aromatic fatty acid can induce preferential HbF production in human erythroid precursors [33] and increase benzidine positivity of K562 cells [34]. Although these agents are reported to be able to activate PPARγ [35,36], in this study, troglitazone reduced both γ-globin and β-globin expression and decreased benzidine positivity, probably via delay of the whole erythroid maturation process.

The differentiation of multipotential hematopoietic progenitors into various lineages is coordinated by lineage-specific transcription factors [37]. The GATA family is a key regulator of erythropoiesis. Expression of GATA-2 precedes that of GATA-1 and decreases as GATA-1 expression increases in order to enable erythroid differentiation [38]. In this study, troglitazone induced sustained expression of GATA-2 mRNA while reducing expression of GATA-1 mRNA in ECFCs. A previous report also showed that troglitazone suppresses expression of GATA-1 in K562 cells [12]. Taken together, these results suggest that troglitazone may delay erythroid maturation by regulating expression of the GATA family through a PPARγ-related signal.

Troglitazone substantially delayed erythroid maturation, but pioglitazone had a weaker effect and 15d-PGJ_2 had no effect. Although PPARγ affinity for 15d-PGJ_2 (Kd = 2 μM) is known to be much lower than that for TZDs (Kd = 30–750 nM), that for pioglitazone is higher than that for troglitazone [2–4,39]. Differences in the potencies for delaying erythroid maturation suggest the possible involvement of unknown PPARγ-related molecular mechanisms. Indeed, among PPARγ ligands reported previously, inhibition of cell proliferation has been achieved predominantly using troglitazone in several cell lines [40–42]. Among the TZDs, only troglitazone contains a vitamin E moiety [43]. The troglitazone-specific effects might be due to its characteristic structure [44].

In conclusion, we demonstrated that PPARγ ligands modulate proliferation and maturation of erythroid progenitor cells. Further studies are needed in order to elucidate the pathways regulating the balance of hematopoiesis via PPARγ-related signals.

Acknowledgments

We thank S. Aoki for excellent technical assistance. We are indebted to Dr. S.B. Krantz (Department of Medicine–Hematology/Oncology, Vanderbilt University School of Medicine, Nashville, TN, USA) for critical reading of the manuscript.

References

1. Mangelsdorf DJ, Thummel C, Beato M, et al. The nuclear receptor superfamily: the second decade. Cell. 1995;83:835–839.
2. Forman BM, Tontonoz P, Chen J, Brun RP, Spiegelman BM, Evans RM. 15-Deoxy-$\Delta^{12,14}$-prostaglandin J_2 is a ligand for the adipocyte determination factor PPARγ. Cell. 1995;83:803–812.
3. Kliewer SA, Lenhard JM, Willson TM, Patel I, Morris DC, Lehmann JM. A prostaglandin J_2 metabolite binds peroxisome proliferator–activated receptor γ and promotes adipocyte differentiation. Cell. 1995; 83:813–819.

4. Lehmann JM, Moore LB, Smith-Oliver TA, Wilkison WO, Willson TM, Kliewer SA. An antidiabetic thiazolidinedione is a high affinity ligand for peroxisome proliferator–activated receptor γ (PPARγ). J Biol Chem. 1995;270:12953–12956.
5. Tontonoz P, Hu E, Spiegelman BM. Stimulation of adipogenesis in fibroblasts by PPARγ2, a lipid-activated transcription factor. Cell. 1994;79:1147–1156.
6. Yanase T, Yashiro T, Takitani K, et al. Differential expression of PPARγ1 and γ2 isoforms in human adipose tissue. Biochem Biophys Res Commun. 1997;233:320–324.
7. Fajas L, Auboeuf D, Raspe E, et al. The organization, promoter analysis, and expression of the human PPARγ gene. J Biol Chem. 1997;272: 18779–18789.
8. Greene ME, Blumberg B, McBride OW, et al. Isolation of the human peroxisome proliferator activated receptor γ cDNA: expression in hematopoietic cells and chromosomal mapping. Gene Expr. 1995;4: 281–299.
9. Greene ME, Pitts J, McCarville MA, et al. PPARγ: observations in the hematopoietic system. Prostaglandins Other Lipid Mediat. 2000;62: 45–73.
10. Konopleva M, Andreeff M. Role of peroxisome proliferator–activated receptor-γ in hematologic malignancies. Curr Opin Hematol. 2002;9: 294–302.
11. Hirase N, Yanase T, Mu Y, et al. Thiazolidinedione induces apoptosis and monocytic differentiation in the promyelocytic leukemia cell line HL60. Oncology. 1999;57(suppl 2):17–26.
12. Hirase N, Yanase T, Mu Y, et al. Thiazolidinedione suppresses the expression of erythroid phenotype in erythroleukemia cell line K562. Leuk Res. 2000;24:393–400.
13. Zang C, Liu H, Posch MG, et al. Peroxisome proliferator–activated receptor γ ligands induce growth inhibition and apoptosis of human B lymphocytic leukemia. Leuk Res. 2004;28:387–397.
14. Gimble JM, Robinson CE, Wu X, et al. Peroxisome proliferator–activated receptor-γ activation by thiazolidinediones induces adipogenesis in bone marrow stromal cells. Mol Pharmacol. 1996;50:1087–1094.
15. Deldar A, Williams G, Stevens C. Pathogenesis of thiazolidinedione induced hematotoxicity in the dog [abstract]. Diabetes. 1993;42:57A. Abstract 179.
16. Williams GD, Deldar A, Jordan WH, Gries C, Long G, Dimarchi RD. Subchronic toxicity of the thiazolidinedione, Tanabe-174 (Ly282449) in the rat and dog [abstract]. Diabetes. 1993;42:59A. Abstract 186.
17. Parulkar AA, Pendergrass ML, Granda-Ayala R, Lee TR, Fonseca VA. Nonhypoglycemic effects of thiazolidinediones. Ann Intern Med. 2001;134:61–71.
18. Sawada K, Krants SB, Kans JS, et al. Purification of human erythroid colony-forming units and demonstration of specific binding of erythropoietin. J Clin Invest. 1987;80:357–366.
19. Sawada K, Krantz SB, Dai CH, et al. Transitional change of colony stimulating factor requirements for erythroid progenitors. J Cell Physiol. 1991;149:1–8.
20. Muta K, Krantz SB, Bondurant MC, Dai CH. Stem cell factor retards differentiation of normal human erythroid progenitor cells while stimulating proliferation. Blood. 1995;86:572–580.
21. Choi I, Muta K, Wickrema A, Krantz SB, Nishimura J, Nawata H. Interferon γ delays apoptosis of mature erythroid progenitor cells in the absence of erythropoietin. Blood. 2000;95:3742–3749.
22. Matsushima T, Nakashima M, Oshima K, et al. Receptor binding cancer antigen expressed on SiSo cells, a novel regulator of apoptosis of erythroid progenitor cells. Blood. 2001;98:313–321.
23. Leesnitzer LM, Parks DJ, Bledsoe RK, et al. Functional consequences of cysteine modification in the ligand binding sites of peroxisome proliferator activated receptors by GW9662. Biochemistry. 2002;41: 6640–6650.
24. Kusukawa N, Uemori T, Asada K, Kato I. Rapid and reliable protocol for direct sequencing of material amplified by the polymerase chain reaction. Biotechniques. 1990;9:66–68.
25. Osawa M, Yamaguchi T, Nakamura Y, et al. Erythroid expansion mediated by the Gfi-1B zinc finger protein: role in normal hematopoiesis. Blood. 2002;100:2769–2777.
26. Smith RD, Li J, Noguchi CT, Schechter AN. Quantitative PCR analysis of HbF inducers in primary human adult erythroid cells. Blood. 2000;95:863–869.
27. Wang M, Tang DC, Liu W, et al. Hydroxyurea exerts bi-modal dose-dependent effects on erythropoiesis in human cultured erythroid cells via distinct pathways. Br J Haematol. 2002;119:1098–1105.
28. Padilla J, Kaur K, Cao HJ, Smith TJ, Phipps RP. Peroxisome proliferator activator receptor-γ agonists and 15-deoxy-$\Delta^{12,14}$-PGJ_2 induce apoptosis in normal and malignant B-lineage cells. J Immunol. 2000;165:6941–6948.
29. Harris SG, Phipps RP. Prostaglandin D_2, its metabolite 15-d-PGJ_2, and peroxisome proliferator activated receptor-γ agonists induce apoptosis in transformed, but not normal, human T lineage cells. Immunology. 2002;105:23–34.
30. Wang LH, Yang XY, Zhang X, et al. Transcriptional inactivation of STAT3 by PPARγ suppresses IL-6-responsive multiple myeloma cells. Immunity. 2004;20:205–218.
31. Sakatoku H, Inoue S. In vitro proliferation and differentiation of erythroid progenitors of cord blood. Stem Cells. 1997;15:268–274.
32. Cao A, Moi P. Regulation of the globin genes. Pediatr Res. 2002; 51:415–421.
33. Fibach E, Prasanna P, Rodgers GP, Samid D. Enhanced fetal hemoglobin production by phenylacetate and 4-phenylbutyrate in erythroid precursors derived from normal donors and patients with sickle cell anemia and β-thalassemia. Blood. 1993;82:2203–2209.
34. Witt O, Mönkemeyer S, Rönndahl G, et al. Induction of fetal hemoglobin expression by the histone deacetylase inhibitor apicidin. Blood. 2003;101:2001–2007.
35. Pineau T, Hudgins WR, Liu L, et al. Activation of a human peroxisome proliferator–activated receptor by the antitumor agent phenylacetate and its analogs. Biochem Pharmacol. 1996;52:659–667.
36. Han S, Wada RK, Sidell N. Differentiation of human neuroblastoma by phenylacetate is mediated by peroxisome proliferator–activated receptor γ. Cancer Res. 2001;61:3998–4002.
37. Orkin SH. Diversification of haematopoietic stem cells to specific lineages. Nat Rev Genet. 2000;1:57–64.
38. Tsai FY, Orkin SH. Transcription factor GATA-2 is required for proliferation/survival of early hematopoietic cells and mast cell formation, but not for erythroid and myeloid terminal differentiation. Blood. 1997; 89:3636–3643.
39. Young PW, Buckle DR, Cantello BC, et al. Identification of high-affinity binding sites for the insulin sensitizer rosiglitazone (BRL-49653) in rodent and human adipocytes using a radioiodinated ligand for peroxisomal proliferator–activated receptor γ. J Pharmacol Exp Ther. 1998;284:751–759.
40. Koga H, Harada M, Ohtsubo M, et al. Troglitazone induces $p27^{Kip1}$-associated cell-cycle arrest through down-regulating Skp2 in human hepatoma cells. Hepatology. 2003;37:1086–1096.
41. Sarraf P, Mueller E, Jones D, et al. Differentiation and reversal of malignant changes in colon cancer through PPARγ. Nat Med. 1998; 4:1046–1052.
42. de Dios ST, Bruemmer D, Dilley RJ, et al. Inhibitory activity of clinical thiazolidinedione peroxisome proliferator activating receptor-γ ligands toward internal mammary artery, radial artery, and saphenous vein smooth muscle cell proliferation. Circulation. 2003;107:2548–2550.
43. Inoue I, Katayama S, Takahashi K, et al. Troglitazone has a scavenging effect on reactive oxygen species. Biochem Biophys Res Commun. 1997;235:113–116.
44. Davies GF, Khandelwal RL, Wu L, Juurlink BH, Roesler WJ. Inhibition of phosphoenolpyruvate carboxykinase (PEPCK) gene expression by troglitazone: a peroxisome proliferator–activated receptor-γ (PPARγ)-independent, antioxidant-related mechanism. Biochem Pharmacol. 2001;62:1071–1079.

Molecular Human Reproduction Vol.11, No.11 pp. 779–784, 2005
Advance Access publication January 3, 2006
doi:10.1093/molehr/gah219

INHA promoter polymorphisms are associated with premature ovarian failure

Sarah E.Harris[1], Ashwini L.Chand[1], Ingrid M.Winship[2], Ksenija Gersak[3], Yoshihiro Nishi[4], ToshihikoYanase[4], Hajime Nawata[4] and Andrew N.Shelling[1,5]

[1]Department of Obstetrics and Gynaecology, [2]Department of Molecular Medicine, University of Auckland, Auckland, New Zealand, [3]Department of Obstetrics and Gynaecology, University Medical Centre, Ljubljana, Slovenia and [4]Department of Medicine and Bioregulatory Science (Third Department of Internal Medicine), Graduate School of Medical Sciences, Kyushu University, Fukuoka, Japan

[5]To whom correspondence should be addressed at: Department of Obstetrics and Gynaecology, Faculty of Medical and Health Sciences, Private Bag 92019, University of Auckland, Auckland, New Zealand. E-mail: a.shelling@auckland.ac.nz

Inhibin is an important glycoprotein that is involved in folliculogenesis. *INHA*, the gene encoding the inhibin alpha subunit, was recently proposed as a candidate for premature ovarian failure (POF), a syndrome that leads to the cessation of ovarian function under the age of 40 years. 70 POF patients and 70 controls were screened for the previously identified *INHA* −16C>T transition mutation. The T allele was found in 31/70 (44.3%) of controls, but only 18/70 (25.7%) of POF patients. This result indicates that the T allele is significantly underrepresented in the POF patient population (Fisher's exact test, two-tail: $P = 0.033$). Sequence analysis of the *INHA* promoter in 50 POF patients and 50 controls identified a highly polymorphic imperfect TG repeat at approximately −300 bp, that consisted of four common haplotypes (A, B, C and D). The −16T allele is linked to the shortest repeat haplotype (haplotype C). Despite the association between haplotype C and POF, no significant difference was found between the promoter activity of a luciferase reporter construct containing haplotype C, and most of the other haplotypes tested. Interestingly, haplotype B failed to show any promoter activity. We conclude that the inheritance of specific *INHA* promoter haplotypes predispose to the development of premature ovarian failure.

Key words: infertility/inhibin/polymorphism/ovarian failure/TG repeat

Introduction

Inhibins are dimeric glycoproteins consisting of a common inhibin alpha subunit (INHA, 14 kDa) covalently linked to one of two related inhibin beta subunits (INHBA, 18 kDa and INHBB, 18 kDa), which respectively form inhibin A and inhibin B. Inhibins were originally isolated from porcine and bovine follicular fluid (Ling *et al.*, 1985; Miyamoto *et al.*, 1985; Rivier *et al.*, 1985; Robertson *et al.*, 1985) and the main production sites are now known to be the granulosa cells in the female and sertoli cells in the male (Vale *et al.*, 1988). Inhibin A and B both inhibit the secretion of FSH, which is involved in the recruitment and development of ovarian follicles during folliculogenesis, but are themselves secreted by the ovarian follicles at different times during the menstrual cycle. Inhibin B levels are highest at the mid-follicular phase, followed by a decline in the late follicular phase (Groome *et al.*, 1994, 1996). The inhibin A levels rise at mid-cycle, indicative of production and secretion from the preovulatory follicle, then rise again during the luteal phase indicative of production by the corpus luteum (Groome *et al.*, 1994, 1996). Therefore, it is proposed that the role of inhibin B is in the recruitment and initiation of folliculogenesis in small preantral follicles, whereas inhibin A has the endocrine role of pituitary FSH suppression. The activins, which stimulate FSH activity, are composed of homo- or heterodimers of the inhibin beta subunits (Ling *et al.*, 1986; Vale *et al.*, 1986). The inhibin subunits are all members of the transforming growth factor (TGF)-β superfamily, a group of molecules that are involved in cell growth and differentiation.

The genes encoding the three inhibin subunits were recently proposed as candidates for premature ovarian failure (POF) due to inhibin's role in the negative feedback control of FSH (Shelling *et al.*, 2000). POF is a syndrome that leads to the cessation of ovarian function under the age of 40 years. It affects 1% of all women and occurs in 0.1% before the age of 30 years (Coulam *et al.*, 1986). POF may result from either a decreased number of follicles being formed during ovarian development, or by an increased rate of follicle loss. Alternatively, follicles may be present, but unresponsive to hormonal stimulation. The most commonly known causes of POF are X-chromosome abnormalities (Shelling, 2000), but in the majority of women, with a normal karyotype, there is no known cause. Approximately 20–30% of women with POF will have other affected female family members, suggesting that an inherited predisposition to the condition is common. We, and others, have identified mutations in a small number of patients, in the genes encoding the FSH receptor (Aittomaki *et al.*, 1995; Beau *et al.*, 1998; Touraine *et al.*, 1999), the LH/choriogonadotrophin receptor (Latronico *et al.*, 1996) and FOXL2 (Harris *et al.*, 2002). We have also identified a coding variant, 769G>A, in the *INHA* gene that results in a non-conservative amino acid change, A257Thr, in 7% of POF patients. This has recently been corroborated by an Italian group, who showed that 4.5% of POF patients and 25% of patients with primary amenorrhoea were heterozygous for the *INHA* variant (Marozzi *et al.*, 2002). This same group also reported an increased prevalence of the C allele of an *INHA* 5′untranslated region (5′UTR) single-nucleotide polymorphism (SNP), 129C>T, in POF

patients, than in a control group. This SNP had previously been shown to be in linkage disequilibrium with a silent coding SNP (675C>T) and not to be linked to dizygotic twinning (Montgomery *et al.*, 2000).

Expression of all three inhibin subunit genes is stimulated by FSH. However, this expression varies several fold in a tissue-specific manner (Meunier *et al.*, 1988), suggesting that the three genes are regulated by different mechanisms. Analysis of the human and murine promoter sequences of these genes corroborates this theory (Feng *et al.*, 1989; Pei *et al.*, 1991; Su and Hsueh, 1992; Dykema and Mayo, 1994; Tanimoto *et al.*, 1996; Ardekani *et al.*, 1998; Yoshida *et al.*, 1998; Debieve and Thomas, 2002). Typical of many housekeeping genes neither *INHA* nor *INHBB* contain either TATA or CCAAT boxes, and the *INHBB* promoter, though not the *INHA* promoter, is GC rich. Human *INHA* transcription is initiated from three transcription start sites, although only the major one is shared by multiple species (Debieve and Thomas, 2002) and an adjacent GA-rich region is believed to play a role in initiating this transcription. An interesting feature of the *INHA* promoter is the presence of an imperfect TG repeat, that is longer in the human than in the mouse or rat. The *INHA* promoter also contains several response elements, including a cAMP response element (CRE), an adjacent steroidogenic factor 1 (SF1) site and AP1 and AP2 sites, suggesting that it is regulated by cAMP. Indeed, several reporter-gene-assay-based studies have shown that an intact CRE element is required for cAMP-induced up-regulation of murine INHA expression (Pei *et al.*, 1991; Su and Hsueh, 1992). The *INHBA* gene is also regulated by cAMP, and like *INHA*, its promoter contains a CRE element and AP1 and AP2 sites and a TG repeat. However, unlike *INHA* and *INHBB*, the *INHBA* promoter has both TATA and CCAAT boxes. Although *INHBB* contains AP2 sites, it has no CRE element in either of its two promoters (that initiate the transcription of 4 kb and 3 kb transcripts) and does not appear to be regulated by cAMP (Dykema and Mayo, 1994; Feng *et al.*, 1995).

The purpose of our study was to characterize the *INHA* 5′UTR/promoter in a cohort of POF patients and normal control samples, to test our hypothesis that promoter sequence variants, leading to altered *INHA* expression levels, are associated with POF.

Materials and methods

Patient information and DNA extraction

Fifty New Zealand and 20 Slovenian women, with POF, were recruited for this study by the Department of Obstetrics and Gynaecology in Auckland, New Zealand, and the Department of Obstetrics and Gynaecology in Ljubljana, Slovenia. POF was defined as cessation of menses for a duration of 6 months or more before the age of 40 years, along with a FSH concentration of >40 IU/l. A complete medical and gynaecological history was taken from each patient as previously described (Shelling *et al.*, 2000). 50 normal control samples were obtained from the general population of New Zealand and 20 from the general population of Slovenia.

Genomic DNA was extracted from 10 ml samples of blood as previously described (Shelling *et al.*, 2000) and 100 ng was used as a template in a PCR.

DNA sequencing of the INHA *promoter region*

Primers were designed that flanked a 1 kb region of the *INHA* promoter (Figure 1) using the primer select module in the DNAStar computer program from Lasergene (1994) (DNASTAR Inc., Madison, WI, USA) and are as follows: INHA5′F: 5′GCTCCCGGCTCGCCTCCTTACC3′ (nucleotides 42262–42284, accession number AC009955) and INHA3′R: 5′CCTGGCCCTGCTAGTGGGGAACTC3′ (nucleotides 43257–43234, accession number AC009955). Reaction conditions were 0.4 μM of each primer, 0.2 mM of each dNTP, 0.625 U *Taq* polymerase, 1× Q solution and 1× PCR buffer (Qiagen GmbH, Hilden, Germany) in a 25 μl total volume. 30 cycles of PCR were performed, consisting of 1 min at 94°C, 1 min at 62°C and 2 min at 72°C, with a final 10 min extension at 72°C.

PCR products to be sequenced were purified using Roche's High Pure PCR Product Purification Kit (Roche Diagnostics GmbH, Mannheim, Germany).

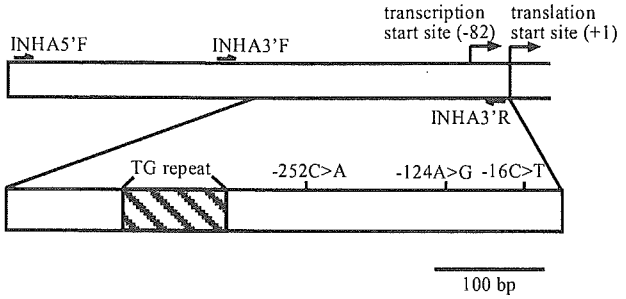

Figure 1. Schematic of *INHA* promoter showing the locations of primers used for sequencing (INHA5′F and INHA3′R) and SSCP (INHA3′F and INHA3′R). The major transcription start site and the translation start are also indicated and all numbering is based on the translation start site, beginning at +1. The region of the promoter that was subcloned to create the pGL3 enhancer constructs is depicted with the TG repeat region shaded and the locations of the −252C>A, −124A>G and −16C>T single-nucleotide polymorphisms (SNPs) are given.

Sequencing reactions were performed using the ABI PRISM™ BIG DYE Terminator Sequencing Kit under standard conditions with an annealing temperature of 55°C. Sequencing products were separated either on a ABI PRISM™ 377 DNA Sequencer XL machine or a ABI PRISM™ 3100 Genetic Analyzer (PE Biosystems, Foster City, CA, USA) at the Centre for Gene Technology, University of Auckland. Primers used for sequencing were INHA5′F and INHA3′R (Figure 1).

Restriction fragment length polymorphism analysis

To rapidly screen all 70 patients and 70 controls for the −16C>T polymorphism an restriction fragment length polymorphism analysis (RFLP) assay was performed as described previously (Montgomery *et al.*, 2000).

Forced restriction fragment length polymorphism analysis

To confirm the sequencing data and to rapidly screen all New Zealand samples for the −124A>G polymorphism, identified in the *INHA* promoter, a forced restriction fragment length polymorphism analysis (FRFLP) assay was devised. Primers were designed to amplify the region of *INHA* promoter containing the polymorphism, such that a *Sau*3AI restriction site was introduced by the reverse primer into samples containing an A at position −124, but not those containing a G. The primers were FRFLPF: 5′AGGTCGCTTGAGGCGAAATCCTTCC3′ and FRFLPR: 5′TCCCACACCCACCCTCTTCTACCCTTCTGA3′.

PCR conditions were as above with the exception that an extension time of 1 min and no Q solution were used. A *Sau*3AI digestion resulted in the 196 bp PCR fragment forming two fragments of 168 bp and 28 bp in the presence of the A allele.

Single-stranded conformation polymorphism

To rapidly screen all New Zealand samples for the polymorphic repeat identified in the INHA promoter, an single-stranded conformation polymorphism (SSCP) assay was used. The region of the promoter containing the repeat was amplified by PCR using primers INHA3′F: 5′TATTGAAAGGGGCCCCAGAAGGTC3′ (nucleotides 42721–42744, accession number AC009955) and INHA3′R. PCR conditions used were the same as for the FRFLP assay. SSCP was performed as described previously (Shelling *et al.*, 2000), using a 14% (w/v) polyacrylamide gel without glycerol.

Construction of reporter genes

To subclone *INHA* promoter regions containing eight different haplotypes, they were amplified from the relevant DNA samples by PCR using the primers: INHAClF: 5′CCGGCTAGCGCTCCCAGGCTCCTG3′, which contains a *Nhe*I restriction site and INHAClR: 5′AGCACTCGAGCTCACCTGGCCCTG3′, which contains a *Xho*I restriction site. PCR conditions used were the same as for the FRFLP assay, with the exception that a proof reading polymerase, Pfu (Promega, Sydney, Australia) plus Q solution was used. The final nucleotide of INHAClR annealed to −16C/T, allowing us, through the use of a proof reading

polymerase, to clone haplotype C with either a C or a T at that position. The PCR products were initially subcloned into pCR®4Blunt-TOPO® (Invitrogen Life Technologies, Carlsbad, CA, USA) according to the manufacturer's instructions. The integrity of the inserts was confirmed by DNA sequencing. The inserts were then released from the vector by a *NheI*/*XhoI* restriction digest and subcloned into pGL3-Enhancer (Promega), upstream of the firefly luciferase gene. The integrity of the inserts were again confirmed by DNA sequencing. Plasmids were propagated in JM109 cells (Promega) and purified using a Plasmid Midi kit (Qiagen).

Transfection of human granulosa cell lines and luciferase assays

A human granulosa cell line (KGN) (Nishi *et al.*, 2001) was plated in a 24 well plate, at a density of 2×10^5 viable cells per well, in Dulbecco's modified Eagle's medium (DMEM)/F12, 10% fetal calf serum (FCS), the day before transfection. Cells were co-transfected with 800 ng of the relevant pGL3-Enhancer construct and 5 ng of the Renilla luciferase control reporter, Promega *Renilla* luciferase-cytomegalovirus (pRL–CMV), diluted in 200 µl DMEM/F12, using 2µl of lipofectamine and 4µl of PLUS reagent (Invitrogen). After 7 h at 37°C, 5% CO_2, 750µl DMEM/F12 and 13.3% FCS were added. After a further 41 h incubation, cells were harvested and luciferase activity determined using the dual-luciferase® reporter assay system (Promega) in a Victor^2 (Wallac, MD, USA), according to manufacturer's instructions. Comparisons between groups were made using one-way analysis of variance (ANOVA).

Results

Initial DNA sequence analysis of the *INHA* promoter identified a polymorphism at position –16C>T. After further analysis, we realized that the –16C>T SNP was identical to the previously identified 129C>T SNP (Montgomery *et al.*, 2000; Marozzi *et al.*, 2002). We use the widely accepted nomenclature guidelines (den Dunnen and Antonarakis, 2000) where the first nucleotide of the translation start codon is labelled as +1. Therefore, the –16C>T variant we have identified probably corresponds to the 129C>T variant reported previously (Montgomery *et al.*, 2000; Marozzi *et al.*, 2002).

Fifty New Zealand and 20 Slovenian POF patients, and the same number of controls, were screened for the –16C>T (Figure 1) transition in the 5′UTR of *INHA*. 29 of 70 (41.4%) controls were heterozygous for this transition and 2 (2.9%) controls were homozygous for T. However, only 18 of 70 (25.7%) POF patients were heterozygous and no T homozygotes were identified. These results indicate that the T allele is significantly underrepresented in the POF patient population (Fisher's exact test, two-tail: $P = 0.033$).

To analyse the *INHA* promoter sequence upstream of the –16C>T SNP, approximately 1 kb fragment of 5′UTR was amplified by PCR and sequenced in 38 of the New Zealand POF patients and 10 of the New Zealand controls. The imperfect TG repeat element located approximately 300 bp upstream of the ATG start site (Figure 1) was found to be highly polymorphic. To determine the exact sequences of both alleles from several of the samples, it was necessary to subclone them into pCR®4Blunt-TOPO® and then sequence using vector primers. Initially, 5 haplotypes were identified [A–D and D(i), Table I]. A –124A>G SNP was also identified and shown to be inherited co-ordinately with the polymorphic repeat, with haplotypes A and B having –124A and haplotypes C, D and D(i), –124G. No other variants were identified. To rapidly type the remaining New Zealand samples, a FRFLP/SSCP combined assay was devised (Figure 2) and all 50 New Zealand POF patients and 50 controls were screened by this method. Where a novel or unclear SSCP pattern was identified, the sample was sequenced and where necessary cloned into pCR®4 Blunt-TOPO® before sequencing. In total, 7 repeat polymorphism haplotypes were typed [A–D and D(i–iii), Table I] along with a third SNP, –252C>A (Figure 1) in one of the control samples (genotype B/C). Haplotype D(i) was found in a single POF patient and haplotypes D(ii) and D(iii) were each identified in single controls. The repeat region varied in length from 94 nucleotides in haplotype A to only 76 nucleotides in haplotype C. Table II details the genotypes identified in both the POF and control populations. Our results indicate that in the New Zealand population, repeat polymorphism haplotype C is in linkage disequilibrium with –16T, as every sample that was heterozygous for –16T was also heterozygous for haplotype C and the control that were homozygous for one was also homozygous for the other. Interestingly, haplotype C contains the shortest repeat polymorphism, being at least 10 nucleotides shorter than the other variants. The C haplotype was underrepresented in the patients (14%), compared to controls (23%) (Table III), however, due to the smaller number of patients following stratification by haplotype, this was not a statistically significant difference. Due to the large number of variables we did not have the statistical power to perform further analyses on this data. With the exception of haplotype C being underrepresented in the POF patients, no other obvious correlation between genotype (haplotype) and phenotype was observed.

To determine whether or not *INHA* promoters containing haplotype C possess significantly different activity to other *INHA* promoters, we made several luciferase reporter constructs which were tested in transient transfection assays. The constructs consisted of *INHA* promoter fragments from approximately –460 to –1, containing the polymorphic TG repeat region, upstream of the luciferase gene (Figure 1). Constructs containing haplotypes A-D, D(i), D(ii) and C with the –252C>A transversion [C(var)] were all created. A mutant version of haplotype C [C(mut)], with a C instead of a T at nucleotide –16, was also made, to distinguish between effects caused by the repeat polymorphism and those caused by the –16 SNP. A human granulosa cell line (KGN) (Nishi *et al.*, 2001), that was determined by RT–PCR to express *INHA* (data not shown), was transfected with either, one of the constructs or the empty reporter vector (pGL3 enhancer) and luciferase activity was measured 48 h after the onset of transfection. Figure 3 shows that the luciferase activities of all constructs, with the exception of B, were approximately 5× higher than that of the empty reporter vector, which was a significant increase in activity (ANOVA, $P = 0.018$). Interestingly, expression levels of construct B were below background luminescence levels (mean reading from six duplicates

Table I. Repeat polymorphisms in the *INHA* promoter

Haplotype	Repeat sequence approximately –300 bp	Length of repeat region	–124 bp	–16 bp
A	$(TG)_8(AG)_5(TG)_6AGAATT(TG)_6AG(TG)_5AG(TG)_5AG(TG)_6$	94	A	C
B	$(TG)_8(AG)_3(TG)_6AGAATT(TG)_6AG(TG)_4AG(TG)_5AG(TG)_6$	88	A	C
C	$(TG)_9(AG)_3(TG)_5AGAATT(TG)_6AG(TG)_5AG(TG)_5$	76	G	T
D	$(TG)_9(AG)_4(TG)_6AGAATT(TG)_6AG(TG)_5AG(TG)_{10}$	90	G	C
D(i)	$(TG)_8(AG)_4(TG)_6(AG)_4(TG)_5AG(TG)_5AG(TG)_{10}$	88	G	C
D(ii)	$(TG)_9(AG)_4(TG)_6AGAATT(TG)_6AG(TG)_5AG(TG)_9$	88	G	C
D(iii)	$(TG)_9(AG)_3(TG)_5AGAATT(TG)_6AG(TG)_5AG(TG)_{10}$	86	G	C

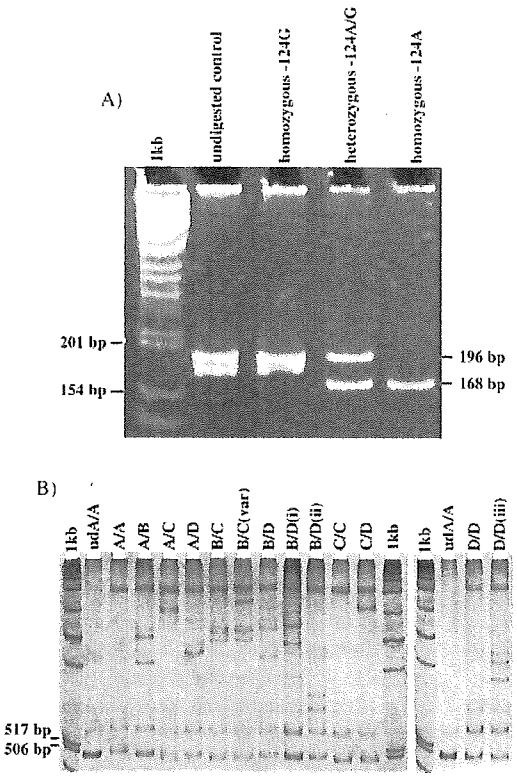

Figure 2. Forced restriction fragment length polymorphism analysis/single-stranded conformation polymorphism (FRFLP/SSCP) analysis of INHA promoter. (**A**) FRFLP analysis of –124A>G using *Sau*3AI. Undigested DNA and digested DNA samples, homozygous for –124G, give a band of 196 bp. DNA samples heterozygous for –124G>A, yield two bands of 196 bp and 168 bp when digested with *Sau*3AI and samples homozygous for –124A a single band of 168 bp. (**B**) SSCP analysis of the TG repeat and –124A>G. An example of each genotype identified in the New Zealand patients and controls is illustrated.

Table II. INHA promoter genotypes in premature ovarian failure (POF) patients and controls

Genotype	Controls	POF patients
A/A	13	13
A/B	5	4
A/C	11	10
A/D	7	12
B/C	4	3
B/D	1	3
B/D(i)	0	1
B/D(ii)	1	0
C/C	1	0
C/D	6	1
D/D	0	3
D/D(iii)	1	0
Total	50	50

taken during three separate experiments, corrected for background reading = –0.034 ± 0.01 SEM), indicating that there was no promoter activity from this construct. The sequence of construct B was reanalysed to confirm its integrity. There was no significant difference (ANOVA, $P = 0.91$) between the luciferase activity measured from the other 7 constructs [constructs A, C, C(var), C(mut), D, D(i) and D(ii)].

Table III. INHA promoter genotypes according to allele in premature ovarian failure (POF) patients and controls

Genotype	Controls	POF patients
A	49	52
B	11	11
C	23	14
D	17	23
Total	100	100

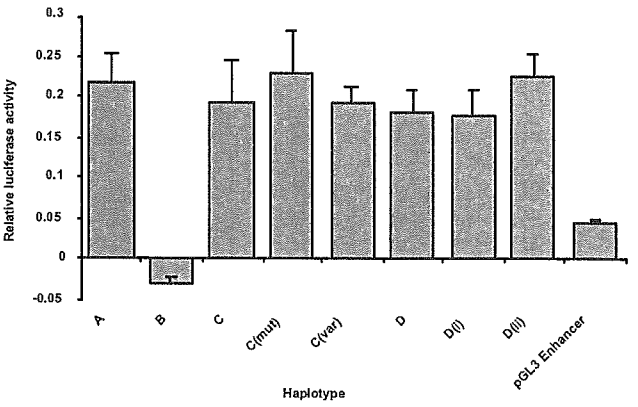

Figure 3. Luciferase activity of the INHA promoter constructs, A, B, C, C(mut), C(var), D, D(i), D(ii) and pGL3 enhancer, 48 h after the onset of transfection. Results are shown as means ± SEM of three independent experiments each performed in duplicate ($n = 6$).

Discussion

Previous studies have revealed the importance of inhibin in follicular development and have shown a strong association between a coding variant, 769G>A, in *INHA*, that causes a non-conservative amino acid change, A257Thr, and POF. More recent studies have identified a pair of linked INHA SNPs, 129C>T and 675C>T (Montgomery *et al.*, 2000). The 129C>T SNP has been associated with susceptibility to POF (Marozzi *et al.*, 2002). We analysed the *INHA* promoter region by DNA sequence analysis, and identified SNP's, including the –16C>T SNP. After further analysis, we realized that the –16C>T SNP was identical to the previously identified 129C>T SNP (Montgomery *et al.*, 2000; Marozzi *et al.*, 2002). The difference in SNP assignment is due to earlier papers (Montgomery *et al.*, 2000; Marozzi *et al.*, 2002) numbering nucleotides from the beginning of the GenBank DNA sequence, rather than the widely accepted nomenclature guidelines (den Dunnen and Antonarakis, 2000) where the first nucleotide of the translation start codon is labelled as +1.

We have screened 70 POF patients and 70 controls from the populations of New Zealand and Slovenia for the –16C>T SNP and detected the T allele in 31 of 70 (44.3%) of the control population, but only 18 of 70 (25.7%) of POF patients, showing a statistically significant difference between the two populations (Fisher's exact test, two-tail: $P = 0.033$). Our findings are similar to those of Marozzi *et al.* (2002) assuming they are the same SNP, as they identified the T allele in 33% of women who experienced physiological menopause and in only 19.7% of POF patients (Marozzi *et al.*, 2002). Overall, we found the T allele at a slightly higher frequency than Marozzi *et al.* (2002) in both control and POF patient populations, and this may be a reflection of either the different populations sampled (Italians versus New Zealanders and Slovenians) or be chance events due to the relatively small

number of samples analysed. Like Marozzi *et al.* (2002) we found that none of the patients in whom we previously identified the 769G>A transition (Shelling *et al.*, 2000) carried a −16T allele. Interestingly, it is the less common variant (−16T) that is underrepresented in the POF patients when compared with the general population. We conclude that the −16T allele represents a susceptibility allele, and protects women from the early development of POF. An alternative presentation of this data is that the −16C allele predisposes women to an early menopause.

Despite the association between the −16C>T SNP and POF, it is unlikely that an SNP located between the transcription and translation start sites, could on its own significantly affect expression from *INHA*. Because the only coding sequence polymorphism that −16C>T was linked to was the silent substitution, 531C>T (675C>T) (Montgomery *et al.*, 2000) we sequenced a approximately 1 kb region of the promoter upstream from this SNP, in 38 New Zealand POF patients and 10 controls to identify any other, potentially more causative variants. The region of promoter sequenced contained several known response elements and had previously been shown to have promoter activity in both human and murine reporter gene assays (Su and Hsueh, 1992; Debieve and Thomas, 2002). From this small initial study we discovered that the extended imperfect TG repeat at approximately −300 is considerably polymorphic in both the POF patient and control populations, with the repeat region ranging from 76 to 94 bp in length and that −16T is linked to the shortest haplotype (haplotype C). Analysis of the remaining New Zealand samples by FRFLP and SSCP confirmed this linkage and lead to the discovery of a total of seven different variants at the repeat locus.

Because −16T is underrepresented in the 70 New Zealand and Slovenian POF patients and is linked to repeat polymorphism haplotype C in the 50 New Zealand POF patients and 50 New Zealand controls, we inferred that the TG repeat polymorphism haplotype C is also underrepresented in the POF patient population. The C haplotype was underrepresented in patients (14%) compared to controls (23%) (Table III), although this was not statistically significant. TG repeats are widely dispersed throughout eukaryotic genomes, with a copy number of approximately 10^5 in the human genome (Hamada *et al.*, 1982; Hamada and Kakunaga 1982). They are associated with the transition from B- to Z-DNA which may be involved in the activation of transcription. Of specific interest, calcium, which was shown to induce a conformational change from B- to Z-DNA in a TG repeat (Dobi and Agoston, 1998), is known to stimulate inhibin production in cultured term placental trophoblast cells (Keelan *et al.*, 1994).

With the exception of haplotype B, the approximately 500 bp region of promoter that was subcloned upstream of the luciferase gene showed an equal level of promoter activity in the KGN cell line, no matter which repeat polymorphism haplotype was present. Haplotype C, despite being underrepresented in the POF patient population, did not have a significantly different level of expression under the conditions used, as might have been predicted. Further investigations are required to determine whether or not the short repeat does indeed alter the expression levels of *INHA* compared to the longer repeats. It is possible that the repeat itself is linked to another polymorphism that is causative in POF and therefore we shall be screening the region of the genome surrounding the *INHA* gene. A study of the mouse *Inha* promoter determined that although a 2.5 kb region upstream of the gene was sufficient to a drive reporter gene in a transgenic mouse, a 6 kb fragment drove expression in pre-antral follicles and in the adrenal glands of immature mice, that was not seen with the 2.5 kb fragment (Hsu *et al.*, 1995). This experiment implied that important regulatory elements are present greater than 2.5 kb upstream from the transcription start site, and therefore warrants further investigation. Future investigations may look at DNA samples from women who have undergone a late menopause to ascertain whether or not −16T/haplotype C is over-represented in this population of women.

The main function of inhibin in women is its regulation of pituitary FSH secretion. It is well established that a decline in serum inhibin levels occurs when ovarian follicular reserves begin to decline, leading to an increase in FSH secretion (Shelling *et al.*, 2000). Because Haplotype C is underrepresented in women with POF, we propose that *in vivo*, *INHA* alleles with haplotype C express a greater amount of INHA than those with other haplotypes. We propose that this leads to an increase in inhibin levels and thus a decrease in FSH levels, which in turn leads to a decrease in the rate of follicle loss, and thus a later menopause. It will be interesting to determine INHA and corresponding FSH levels in the serum of women to see if there is a correlation with different *INHA* promoter genotypes.

Surprisingly, haplotype B showed no promoter activity. Despite careful scrutiny of the construct sequence, no mutations could be detected. There was no obvious reason why haplotype B should have no promoter activity, although we did note that despite being present in 22% of our samples, no haplotype B homozygotes were detected.

In summary we have shown that the imperfect TG repeat in the *INHA* promoter is highly polymorphic and that the shortest repeat (haplotype C) is linked to −16T, which is underrepresented in POF patients compared to normal controls. Under the conditions used in our experiments we failed to demonstrate that haplotype C conveyed a significantly different promoter activity to the *INHA* promoter, compared to the majority of other haplotypes tested. This work underlines the importance of inhibin in the regulation of follicle loss, and indicates that variation in the *INHA* promoter may predispose to premature ovarian failure.

Acknowledgements

We thank the POF patients for their involvement in this study. We also thank the many clinicians who provided these patients. Funding was provided by the University of Auckland Research Committee, the Health Research Council of New Zealand and the Auckland Medical Research Foundation.

References

Aittomaki K, Lucena JL, Pakarinen P, Sistonen P, Tapanainen J, Gromoll J, Kaskikari R, Sankila EM, Lehvaslaiho H, Engel AR et al. (1995) Mutation in the follicle-stimulating hormone receptor gene causes hereditary hypergonadotropic ovarian failure. Cell 82,959–968.

Ardekani AM, Romanelli JC and Mayo KE (1998) Structure of the rat inhibin and activin betaA-subunit gene and regulation in an ovarian granulosa cell line. Endocrinology 139,3271–3279.

Beau I, Touraine P, Meduri G, Gougeon A, Desroches A, Matuchansky C, Milgrom E, Kuttenn F and Misrahi M (1998) A novel phenotype related to partial loss of function mutations of the follicle stimulating hormone receptor. J Clin Invest 102,1352–1359.

Coulam CB, Adamson SC and Annegers JF (1986) Incidence of premature ovarian failure. Obstet Gynecol 67,604–606.

Debieve F and Thomas K (2002) Control of the human inhibin alpha chain promoter in cytotrophoblast cells differentiating into syncytium. Mol Hum Reprod 8,262–270.

den Dunnen JT and Antonarakis SE (2000) Mutation nomenclature extensions and suggestions to describe complex mutations: a discussion. Human Mutation 15,7–12.

Dobi AV and Agoston D (1998) Submillimolar levels of calcium regulates DNA structure at the dinucleotide repeat (TG/AC)n. Proc Natl Acad Sci USA 95,5981–5986.

Dykema JC and Mayo KE (1994) Two messenger ribonucleic acids encoding the common beta B-chain of inhibin and activin have distinct 5′-initiation sites and are differentially regulated in rat granulosa cells. Endocrinology 135,702–711.

Feng ZM, Li YP and Chen CL (1989) Analysis of the 5′-flanking regions of rat inhibin alpha- and beta-B-subunit genes suggests two different regulatory mechanisms. Mol Endocrinol 3,1914–1925.